Transcription and splicing dynamics during early *Drosophila* development

PEDRO PRUDÊNCIO,[1,2,5] ROSINA SAVISAAR,[1,5] KENNY REBELO,[1,4,5] RUI GONÇALO MARTINHO,[1,2,3] and MARIA CARMO-FONSECA[1]

[1]Instituto de Medicina Molecular João Lobo Antunes, Faculdade de Medicina, Universidade de Lisboa, 1649-028 Lisboa, Portugal

[2]Algarve Biomedical Center Research Institute (ABC-RI), Universidade do Algarve, 8005-139 Faro, Portugal

[3]Department of Medical Sciences and Institute for Biomedicine (iBiMED), Universidade de Aveiro, 3810-193 Aveiro, Portugal

ABSTRACT

Widespread cotranscriptional splicing has been demonstrated from yeast to human. However, most studies to date addressing the kinetics of splicing relative to transcription used either *Saccharomyces cerevisiae* or metazoan cultured cell lines. Here, we adapted native elongating transcript sequencing technology (NET-seq) to measure cotranscriptional splicing dynamics during the early developmental stages of *Drosophila melanogaster* embryos. Our results reveal the position of RNA polymerase II (Pol II) when both canonical and recursive splicing occur. We found heterogeneity in splicing dynamics, with some RNAs spliced immediately after intron transcription, whereas for other transcripts no splicing was observed over the first 100 nt of the downstream exon. Introns that show splicing completion before Pol II has reached the end of the downstream exon are necessarily intron-defined. We studied the splicing dynamics of both nascent pre-mRNAs transcribed in the early embryo, which have few and short introns, as well as pre-mRNAs transcribed later in embryonic development, which contain multiple long introns. As expected, we found a relationship between the proportion of spliced reads and intron size. However, intron definition was observed at all intron sizes. We further observed that genes transcribed in the early embryo tend to be isolated in the genome whereas genes transcribed later are often overlapped by a neighboring convergent gene. In isolated genes, transcription termination occurred soon after the polyadenylation site, while in overlapped genes, Pol II persisted associated with the DNA template after cleavage and polyadenylation of the nascent transcript. Taken together, our data unravel novel dynamic features of Pol II transcription and splicing in the developing *Drosophila* embryo.

Keywords: *Drosophila melanogaster* embryo; NET-seq; transcription termination; splicing kinetics

INTRODUCTION

It is by now largely accepted that splicing can happen, and often does happen, while transcription is still in progress (Beyer and Osheim 1988; Carrillo Oesterreich et al. 2010; Ameur et al. 2011; Khodor et al. 2011; Windhager et al. 2012; Brugiolo et al. 2013; Nojima et al. 2015; Alpert et al. 2017). It is also known that the processes of splicing and transcription are tightly interlinked. The RNA polymerase II (Pol II) elongation rate can affect exon inclusion (de la Mata et al. 2003; Fong et al. 2014; Aslanzadeh et al. 2018; Maslon et al. 2019), and many of the proteins involved in splicing associate with the Pol II large subunit carboxy-terminal domain (CTD) (Morris and Greenleaf

2000; Emili et al. 2002; David et al. 2011; Görnemann et al. 2011; Hsin and Manley 2012; Nojima et al. 2018). Conversely, splicing may also affect transcription, with evidence suggesting that Pol II slows down at exons (Alexander et al. 2010; Carrillo Oesterreich et al. 2010; Jonkers et al. 2014; Veloso et al. 2014; Mayer et al. 2015), potentially to allow for splicing to complete.

Several studies have addressed the timing of intron excision relative to Pol II elongation. A nascent RNA sequencing study (Carrillo Oesterreich et al. 2016) showed that in *Saccharomyces cerevisiae*, splicing could occur as soon as the 3′ splice site had emerged from the transcription machinery, suggesting that splicing may be completed immediately after intron transcription. Previous attempts to determine the duration of splicing in vivo had returned estimates ranging from a few seconds to several minutes (Alpert et al. 2017). The lowest of these estimates, such as the few-second estimate reported in Martin et al. (2013), are consistent with

[4]**Present address:** Donnelly Centre, University of Toronto, Toronto, Ontario M5S 3E1, Canada

[5]These authors contributed equally to this work.

Corresponding authors: carmo.fonseca@medicina.ulisboa.pt, rgmartinho@ua.pt

splicing being completed right after the 3′ splice site is transcribed. The most recent breakthroughs in the field followed the development of long-read nascent RNA sequencing technologies (Drexler et al. 2020; Reimer et al. 2021; Sousa-Luís et al. 2021). Collectively, these studies performed in human and *Drosophila* cultured cell lines show that although many introns are immediately excised as soon as the downstream exon emerges from Pol II, a subset remains unspliced and progressively undergoes delayed splicing while Pol II transcribes further (Drexler et al. 2020; Reimer et al. 2021; Sousa-Luís et al. 2021).

Here, we studied the dynamic properties of transcription and cotranscriptional splicing during the early stages of development in *Drosophila melanogaster* embryos using native elongating transcript sequencing (NET-seq) (Churchman and Weissman 2011; Nojima et al. 2015). An advantage of using *Drosophila* embryos is that they are more physiological than cultured cell lines. Moreover, compared to human, the *Drosophila* genome is more compact (Graveley et al. 2011) and thus the coverage of NET-seq reads on intragenic regions is higher. Another advantage of the *Drosophila* model is that genes transcribed initially in the embryo have few and short introns (like yeast genes), whereas genes transcribed later contain multiple long introns (more similar to human genes). An additional feature of *Drosophila* is the presence of many genes with exceptionally long introns that are subdivided by a noncanonical mechanism termed recursive splicing (Duff et al. 2015; Joseph et al. 2018; Pai et al. 2018). For all these reasons, *Drosophila* is an attractive model to study cotranscriptional splicing dynamics.

Drosophila early development is characterized by rapid mitotic cycles that lack cytokinesis, resulting in nuclear proliferation in a syncytial cytoplasm (Campos-Ortega 1985; Laver et al. 2015). During these initial mitotic divisions, which impose significant constraints on transcription and splicing (Shermoen and O'Farrell 1991; Rothe et al. 1992; Guilgur et al. 2014; Martinho et al. 2015; Sandler et al. 2018; Kwasnieski et al. 2019), the embryo largely relies on maternally deposited mRNAs. Subsequently, the duration of the cell cycle is progressively expanded, membranes form between the nuclei and segregate them into cells, and the zygotic transcriptome starts to be fully expressed (Campos-Ortega 1985; Blythe and Wieschaus 2015; Yuan et al. 2016). By performing *d*NET-seq in the developing *Drosophila* embryo, we have unraveled novel dynamic features of Pol II transcription and splicing.

RESULTS

Native elongating transcript sequencing in *Drosophila* embryos (*d*NET-seq)

Our first task was to adapt the NET-seq technology for use in *Drosophila* embryos (henceforth referred to as *d*NET-

seq). The NET-seq technique involves isolation of transcription complexes formed by Pol II, the DNA template and the nascent RNA by immunoprecipitation, without crosslinking (Churchman and Weissman 2011; Nojima et al. 2015). After solubilization of Pol II complexes under native conditions by extensive micrococcal nuclease (MNase) digestion of isolated native chromatin, elongation complexes were immunoprecipitated using antibodies that specifically recognize different phosphorylation states of the Pol II CTD (Nojima et al. 2015).

We collected embryos at 2–3 h after fertilization (referred to as early embryos) and 4–6 h after fertilization (referred to as late embryos) (Fig. 1A). Analysis of embryos stained with a fluorescent dye to visualize DNA (Fig. 1B) revealed that early embryos were predominantly in mitotic cycle 14 (stage 5), which is when massive activation of zygotic transcription occurs (Campos-Ortega 1985; Laver et al. 2015). The majority of late embryos were in the late stage of germ-band extension (stage 10; Fig. 1C), when the embryo trunk (also known as the germ-band) elongates in the antero-posterior axis and narrows in the dorso-ventral axis (Campos-Ortega 1985; Laver et al. 2015).

In adapting mNET-seq to *Drosophila* embryos, we optimized buffers and washing conditions to purify the chromatin fraction from manually sorted embryos, solubilize the transcription complexes with MNase digestion and immunoprecipitate Pol II with antibodies. We used rabbit polyclonal antibodies raised against synthetic peptides of the YSPTSPS repeat of the CTD of the largest Pol II subunit in *Saccharomyces cerevisiae*, phosphorylated at either S5 (ab5131 Abcam) or S2 (ab5095 Abcam). Both antibodies have been extensively used for chromatin immunoprecipitation experiments in *Drosophila melanogaster* (Yan et al. 2014; Dahlberg et al. 2015; Lee et al. 2015; Boija et al. 2017; Vizcaya-Molina et al. 2018; Akhtar et al. 2019; Arzate-Mejía et al. 2020).

To enable directional sequencing, the 5′ hydroxyl (OH) generated by MNase digestion of RNA was first converted to a 5′ phosphate by T4 polynucleotide kinase (Fig. 1D). RNA was then purified from the immunoprecipitated Pol II complexes and size-selected using an RNA purification kit procedure that combines a unique buffer system with a column technology (see the Materials and Methods section for more detail). RNAs with a size above 60 nt were used for subsequent ligation of specific adapters to the 5′ P and 3′ OH ends of each RNA fragment followed by PCR-based preparation of a cDNA library for high-throughput Illumina sequencing (Fig. 1D). After sequencing, adapter sequences were trimmed and paired-end reads with sequence overlaps were merged into a single read that spans the full length of the original RNA fragment (dark orange; Fig. 1E). The resulting single reads were aligned to the *Drosophila* reference genome. The nucleotide at the 3′ end of each RNA fragment was identified and its genomic position recorded (asterisk; Fig. 1E).
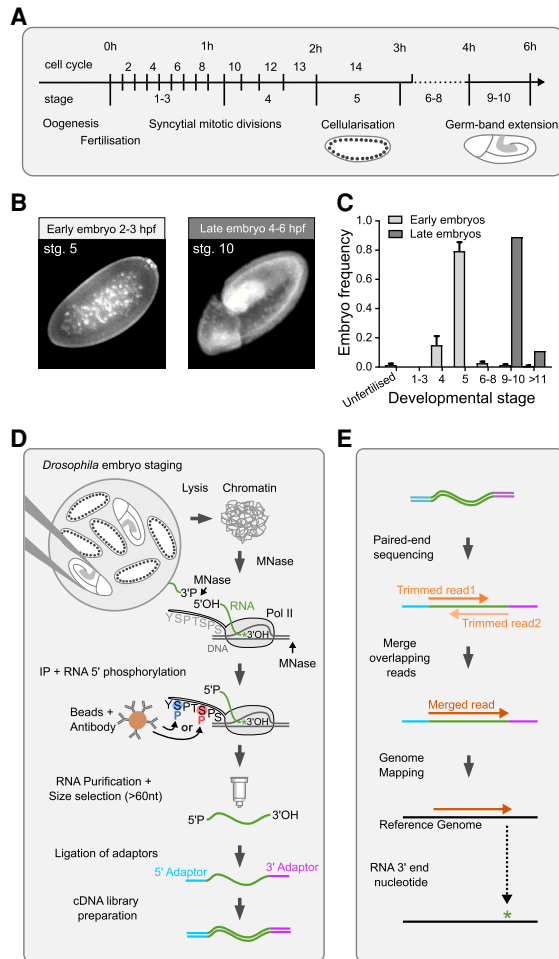
FIGURE 1. Native elongating transcript sequencing in *Drosophila* embryos. (*A*) Timeline of *Drosophila* early embryonic development, which starts with 13 rapid syncytial mitotic cycles. During interphase of cycle 14, membranes form between the nuclei located at the periphery of the embryo (cellularization). The new cells start morphogenetic movements leading to elongation of the embryo trunk (germband extension). (*B*) Representative images (stained for DNA) of embryos in mitotic cycle 14 (stage 5) and late germ-band expansion (stage 10). (*C*) The graph depicts the developmental stage of embryos sorted into the "early" and "late" groups. Approximately 30,000 early embryos and 15,000 late embryos were analyzed. (*D*) Outline of the *d*NET-seq experimental protocol. (*E*) Outline of *d*NET-seq data analysis.

Two to three *d*NET-seq libraries were independently prepared from early and late embryos using S5P antibody; three additional libraries were prepared from late embryos using S2P antibody. Each library was sequenced to a high coverage with a read length of 150 bp (Supplemental Fig. S1; see the Materials and Methods section for more detail). Experimental reproducibility was demonstrated by strong agreement of uniquely aligned read density between biological replicates prepared with antibodies raised against the CTD phosphorylated on either serine 5 (S5P) or serine 2 (S2P) positions (Supplemental Fig. S1B–E). This suggests

that both S5P and S2P antibodies recognize the CTD of elongating Pol II in *Drosophila* embryos.

*d*NET-seq captures splicing intermediates and spliceosomal snRNAs

NET-seq captures not only the final (3′ OH end) nucleotide of nascent RNA but also the 3′ OH end of RNAs that associate with the Pol II elongation complex (Nojima et al. 2015, 2018; Schlackow et al. 2017). Notably, in humans, mNET-seq of Pol II phosphorylated on CTD serine 5 detected splicing intermediates formed by cleavage at the 5′ splice site after the first splicing reaction. The presence of such intermediates manifests as an enrichment of reads whose 3′ ends map precisely to the last nucleotide of an exon. In both early and late *Drosophila* embryos, we indeed observed large peaks of *d*NET-seq/S5P reads mapping to the last nucleotide of spliced exons, as shown for the *kuk* gene (green asterisk; Fig. 2A). We also detected *d*NET-seq/S5P peaks at the last nucleotide of introns, as shown for the *eEF1alpha1* gene (pink asterisk; Fig. 2B); enrichment for these reads results from coimmunoprecipitation of released intron lariats after completion of the splicing reaction (Fig. 2B). In addition, we observed reads corresponding to mature snRNAs engaged in cotranscriptional spliceosome assembly, suggesting that *d*NET-seq was capturing the free 3′ OH ends of the snRNAs (blue asterisk; Fig. 2C). We found prominent peaks at the end of spliceosomal U1, U2, U4, and U5 snRNAs. As expected, no peak was detected mapping to the end of the U3 snRNA, which is involved in the processing of pre-rRNA synthesized by Pol I. Noteworthy, we observed an accumulation of *d*NET-seq signal at the end of U6 snRNA (Supplemental Fig. S2A), contrasting with a lack of peak observed in mammalian cells (Nojima et al. 2018). This is consistent with the finding that most mammalian U6 snRNAs contain a 2′,3′-cyclic phosphate terminal group at the 3′ end, whereas U6 3′ ends in *Drosophila* cells consist of either a cyclic 2′,3′-phosphate, a 3′-phosphate or a 2′,3′-hydroxyl group (Lund and Dahlberg 1992).

To quantify how many constitutively spliced exons have *d*NET-seq peaks at the end, we applied an algorithm that finds nucleotides where the NET-seq read density is at least three standard deviations above the transcript mean in a local region defined by 100 bp upstream and downstream (Churchman and Weissman 2011; Prudêncio et al. 2020). Upon analyzing replicates of *d*NET-seq/S5P and *d*NET-seq/S2P libraries, we identified over 10,000 exons showing splicing intermediate peaks (Fig. 2D). As peaks were more frequently detected on exons of genes with higher read density (Supplemental Fig. S2B), we classified the exons into four groups (quartiles) based on the *d*NET-seq read density of the corresponding gene and restricted the analysis to exons in the fourth quartile, that is, from genes with the highest read density.
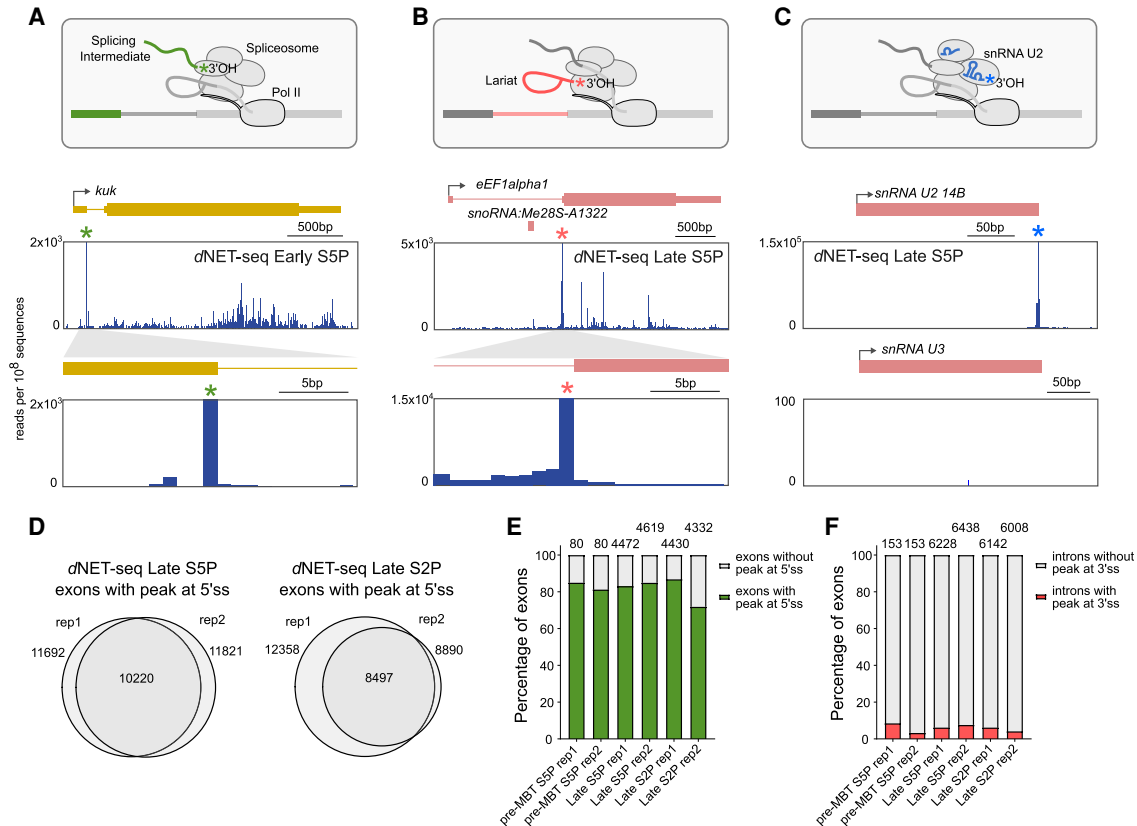
FIGURE 2. *d*NET-seq captures splicing intermediates and spliceosomal snRNAs. (*A–C*) The diagrams outline the 3′ OH ends generated by cotranscriptional cleavage at the 5′ splice site (*A*), the 3′ splice site (*B*), and the free 3′ OH end of spliceosomal snRNAs (*C*). *Below* each diagram, *d*NET-seq/S5P profiles over the indicated genes are depicted (data from late embryos). The green asterisk denotes the peak at the end of the exon (*A*). The pink asterisk denotes the peak at the end of the intron (*B*). The blue asterisk denotes the peak at the end of the U2 snRNA gene (*C*). Arrows indicate the direction of transcription. Exons are represented by boxes. Thinner boxes represent UTRs. Introns are represented by lines connecting the exons. (*D*) Comparison (Venn diagrams) of exons with a splicing intermediate peak detected in biological replicates of *d*NET-seq/S5P and *d*NET-seq/S2P libraries. (*E,F*) Frequency of peaks corresponding to splicing intermediates (*E*) and released intron lariats (*F*) in pre-MBT genes and genes expressed in late embryos. Only genes with the highest read density (fourth quartile) were considered.

The results show that splicing intermediate peaks are detected in ∼80% of all constitutively spliced exons. We further analyzed the so-called pre-MBT (mid-blastula transition) genes, which are the first zygotic genes to become transcriptionally active in early embryos (Chen et al. 2013), and genes expressed in late embryos. We found similar proportions of splicing intermediate peaks associated with pre-MBT and late genes in the S5P and the S2P data sets (Fig. 2E). We then used the same methodology and the same set of genes to detect peaks at the last intronic nucleotide, corresponding to released intron lariats. Such peaks were detected in <10% of introns (Fig. 2F).

Taken together, these results demonstrate that *d*NET-seq with antibodies that recognize the Pol II CTD phosphorylated at either S5 or S2 positions is capable of detecting splicing intermediates and spliceosomal snRNAs in *Drosophila* embryos, as previously reported in mammalian cells (Nojima et al. 2015, 2018; Schlackow et al. 2017).

*d*NET-seq specifically captures nascent RNA

To validate that we were detecting nascent transcription in *Drosophila* embryos, we analyzed maternal mRNAs that are transcribed during oogenesis and loaded into the egg (Fig. 3A). As expected, maternal transcripts such as *bicoid* (Fig. 3B), *nanos* (Supplemental Fig. S3A), *gurken* (Supplemental Fig, S3B), and *Rab32* (Supplemental Fig. S3C) were detected by RNA-seq in embryos collected 2–3 h after fertilization, but the *d*NET-seq signal over these genes was negligible. However, a robust *d*NET-seq/S5P signal was found at the *pumilio* gene (Fig. 3C). Expression of this gene was considered to be exclusively maternal based on RNA-seq (Lott et al. 2011) and Pol II ChIP-seq data (Chen et al. 2013), but a GRO-seq study detected *pumilio* nascent transcripts in embryos collected 2–2.5 h postfertilization (Saunders et al. 2013). The detection of *pumilio* RNA in early embryos by GRO-seq and *d*NET-seq/S5P highlights the sensitivity of these two techniques in capturing low-level nascent transcripts.
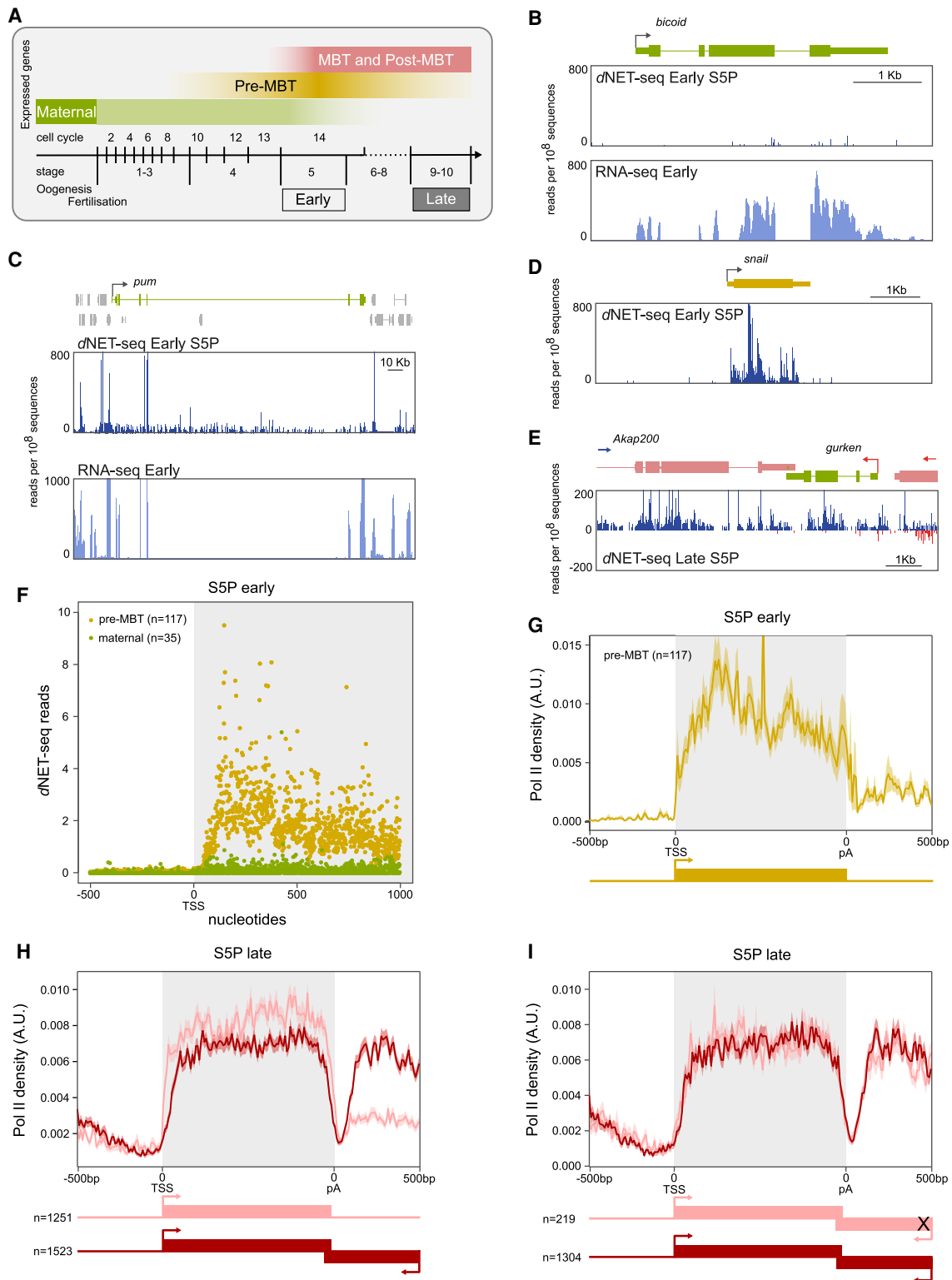
FIGURE 3. *d*NET-seq profiles in early and late embryos. (*A*) The diagram illustrates the temporal expression of maternal, pre-MBT, MBT, and post-MBT genes during *Drosophila* embryonic development. *d*NET-seq/S5P and RNA-seq profiles over the maternal genes *bicoid* (*B*) and *pumilio* (*pum*) (*C*), the pre-MBT gene *snail* (*D*), and the post-MBT gene *Akap200* (*E*). Reads that aligned to the positive strand are in blue, and reads that aligned to the negative strand are in red. (*F*) Meta-analysis of mean *d*NET-seq/S5P read density around the transcription start site (TSS) in maternal and pre-MBT genes (replicate 1). (*G*–*I*) Normalized metagene analysis in arbitrary units (A.U.). The *d*NET-seq/S5P signal is depicted along the normalized gene length (gray background), as well as 500 bp upstream of the transcription start site (TSS) and 500 bp downstream from the polyadenylation (pA) site. (*G*) Pre-MBT genes in early embryos. (*H*) Transcriptionally active genes in late embryos; the signal over genes that have the 3′-UTR overlapped by an antisense gene is depicted in dark red, while the signal over genes with no other genes within 500 bp is depicted in light red. (*I*) Transcriptionally active genes in late embryos; the signal over genes that have the 3′-UTR overlapped by a transcriptionally active antisense gene is depicted in dark red, while the signal over genes with the 3′-UTR overlapped by a transcriptionally inactive antisense gene is depicted in light red.

The stage at which the embryo switches from relying on maternally deposited mRNAs and proteins to undergoing its own transcription is termed the mid-blastula transition (MBT). However, a few genes (known as pre-MBT genes) become transcriptionally active before MBT (Kwasnieski et al. 2019). A strong *d*NET-seq signal was detected in early embryos over the bodies of pre-MBT genes such as *snail* (Fig. 3D), *fushi tarazu* (Supplemental Fig. S3D) and *odd skipped* (Supplemental Fig. S3E). Altogether, we examined 117 previously identified pre-MBT genes and 35 maternal mRNAs (Fig. 3F; Supplemental Fig. S3F). The finding that a robust *d*NET-seq/S5P signal was recovered from zygotically but not from maternally expressed transcripts indicates that *d*NET-seq is specifically targeting the nascent transcriptome.

*d*NET-seq reveals differences in transcription termination profiles between genes expressed in early and late embryos

Having confirmed that *d*NET-seq was capturing nascent RNA, we next investigated the distribution of Pol II density over transcript regions in early and late embryos. *d*NET-seq/S5P profiles (Fig. 3C–E; Supplemental Fig. S3A–E) do not show the characteristic higher read density near the promoter, as previously described in mammalian cells (Mayer et al. 2015; Nojima et al. 2015). This is most likely because Pol II typically pauses ~30–60 bp downstream from the transcription start site (TSS) (Kwak et al. 2013) and in our *d*NET-seq approach we enrich for RNAs longer than 60 nt (Supplemental Fig. S1F); thus, we only record the position of polymerases that have transcribed at least 60 bp past the TSS.

We then turned our attention to the *d*NET-seq signal around the polyadenylation (pA) site. We found that in pre-MBT genes such as *snail* (Fig. 3D), *tailless (tll)* (Supplemental Fig. S4A), and *nullo* (Supplemental Fig. S4B), the *d*NET-seq/S5P signal ends soon after the pA site. In contrast, genes expressed in late embryos such as *Akap200* (Fig. 3E), *His3.3A* (Supplemental Fig. S3H) and *tsr* (Supplemental Fig. S3I), have a widespread *d*NET-seq/S5P signal on introns and regions downstream from the pA site. Analysis of RNA-seq data sets revealed that mRNAs encoded by these genes are efficiently spliced and 3′-end processed (Supplemental Fig. S3H,I). Thus, *d*NET-seq/S5P is capturing newly synthesized transcripts that have not yet been spliced, as well as RNAs synthesized by Pol II complexes that continued to transcribe the DNA template after the mRNA was cleaved and polyadenylated at the pA site. We further noted that the 3′-UTR of genes with a *d*NET-seq signal extending past the pA site is overlapped by another gene (*gurken*, *Nepl3*, and *IntS1*, respectively), which is transcribed in the opposite direction.

Next, we generated *d*NET-seq metaprofiles for pre-MBT and late genes. Metagene analysis of the *d*NET-seq/S5P

signal on pre-MBT genes expressed in early embryos confirmed that in this group of genes, the *d*NET-seq signal is sharply reduced past the pA site (Fig. 3G). The majority (65) of pre-MBT genes are isolated in the genome, with no other gene on either strand within a region of 500 bp downstream from the pA site, as shown for *tailless (tll)* (Supplemental Fig. S4A). Another 26 pre-MBT genes are embedded in larger genes, as shown for *nullo*, which is located within a long intron of the *CG12541* gene (Supplemental Fig. S4B). A smaller group of pre-MBT genes (21) have neighboring genes located on either strand within a region of 500 bp downstream from the pA site, as shown for *Elba2* (Supplemental Fig. S4C). We further identified 5 pre-MBT genes that have the 3′-UTR overlapped by an antisense convergent gene, as shown for *spook (spo)* (Supplemental Fig. S4D). Notably, in these genes, the *d*NET-seq/S5P signal extended past the pA site (Supplemental Fig. S4C,D).

To identify all the genes that are transcriptionally active in late embryos, we used a strategy adapted from GRO-seq analysis (Core et al. 2008) that relies on read density in gene desert regions as background reference for absence of transcription. Very large intergenic regions (gene deserts) were divided into 50 kb windows, and read densities were calculated by dividing read counts in each window by the window length in bp (Supplemental Fig. S4E). Genes with *d*NET-seq signal over the gene body (in RPKM) above the 90th percentile of read density for all intergenic regions analyzed were considered to be transcriptionally active (Supplemental Fig. S4F). We identified ~7000 active genes, with similar results obtained from *d*NET-seq/S5P and *d*NET-seq/S2P data sets (Supplemental Fig. S4G). This set of active genes includes over 85% of the 3500 genes previously identified as actively transcribed after the mid-blastula transition (MBT) based on ChIP-seq experiments (Chen et al. 2013). Next, we divided the genes transcribed in late embryos into two groups, depending on whether their 3′-UTR was or was not overlapped by another convergent gene. The metagene analysis shows that when averaged across all transcribed genes, a very low *d*NET-seq signal is detected at the pA site (Fig. 3H; Supplemental Fig. S3G), as expected assuming that when Pol II reaches this site, the nascent transcript is cleaved and polyadenylated and therefore there is no RNA left attached to the polymerase to be sequenced. However, in the case of late genes that have the 3′-UTR overlapped by an antisense (convergent) gene, the *d*NET-seq/S5P and *d*NET-seq/S2P signals increase again after the pA site (Fig. 3H; Supplemental Fig. S3G). Using the methodology described above to identify transcribed genes, we found that the vast majority (>80%) of overlapping convergent genes were transcriptionally active and only 219 genes were silent. The metagene analysis shown in Figure 3I clearly indicates that the detection of *d*NET-

seq/S5P signal past the pA site is independent from transcription of the convergent overlapping gene.

In conclusion, the distribution profiles of *d*NET-seq/S5P and *d*NET-seq/S2P reads around the pA site suggest distinct patterns of transcription termination for genes that are either isolated in the genome or overlapped by another convergent gene. However, we cannot exclude the possibility that specifically in isolated genes, the lack of *d*NET-seq signal results from loss of CTD phosphorylation as Pol II transcribes past the pA site.

Analysis of *d*NET-seq read density profiles

We next focused on the distribution of *d*NET-seq reads on exons and introns. The number of nascent RNA reads whose 3′ ends map at a particular genomic position is proportional to the number of Pol II molecules at that position. Thus, Pol II pause sites can be detected as local peaks in NET-seq read density (Churchman and Weissman 2011; Larson et al. 2014). However, because we performed *d*NET-seq with antibodies that recognize the Pol II CTD phosphorylated at either S5 or S2 positions, changes in read density may reflect dynamic phosphorylation of the CTD rather than Pol II pausing. We excluded signal resulting from splicing intermediates (i.e., reads that map to the very last nucleotide of introns and exons were discarded) in order to analyze only reads whose 3′ ends associate with the Pol II active site. We analyzed both S5P and S2P data. However, we were particularly interested in exploring the multiple peaks of dNET-seq/S5P signal observed on both exons and introns (Fig. 4A), because cotranscriptional splicing has been linked to S5P in humans (Nojima et al. 2015).

A difficulty when performing the systematic identification of *d*NET-seq peaks is that transcripts with higher initiation rates will contain more reads and thus peaks are more likely to be detected than in more lowly transcribed genes. To control for this confound, we developed a peak calling algorithm that detects regions where the local read density is significantly higher than expected by chance, given the over-all read density of the transcript (Fig. 4A; see also the Materials and Methods section). We emphasize that for detecting reads corresponding to splicing intermediates (Fig. 2D–F), we used a peak calling method that looks for significant single-nucleotide positions (Churchman and Weissman 2011), whereas this new method detects higher read regions of variable length.

We then aligned exons and introns on the splice sites and calculated the average peak density at each position. Exons have a higher over-all peak density than introns (mean proportion of nucleotides in peaks ~0.022/~0.015 for replicate 1/replicate 2 introns and ~0.043/~0.034 for replicate 1/replicate 2 exons; $P < 2.2 \times 10^{-16}$ for both replicates; two-tailed Mann–Whitney U-test with the peak densities of individual introns/exons as data points) (Fig.

4B). This is consistent with previous reports indicating that the Pol II elongation rate is decreased over exons in mammalian (Jonkers et al. 2014; Mayer et al. 2015) and *Drosophila* cells (Kwak et al. 2013). In addition, peak density is sharply increased around the 5′ splice site (Fig. 4C). This could indicate either Pol II pausing or increased S5 phosphorylation associated with splice site recognition. We also cannot exclude that misaligned splicing intermediate reads are contributing to the observed increase in peak density around the 5′ splice site. The *d*NETseq/S5P profile around the 3′ splice site shows a higher peak density region just after the intron-exon boundary, and a progressive increase in average exonic peak density is further observed starting roughly 60 nt after the 3′ splice site (Fig. 4C). A very similar peak density metaprofile is observed with the *d*NETseq/S2P data set (Fig. 4D).

A potential caveat of read density analysis is that nucleotide composition varies systematically across exons and introns. For example, exons tend to have a higher GC content than introns (Zhu et al. 2009). This could be problematic as NET-seq relies on MNase digestion of DNA and RNA to solubilize chromatin. MNase digestion of DNA is known to be sequence-biased, with most notably a preference for cleaving just 5′ of an adenine (Dingwall et al. 1981; Hörz and Altenburger 1981; Gaffney et al. 2012). An analysis of the 5′ ends of our reads revealed similar biases for MNase digestion of RNA (Fig. 4D). This sequence preference could lead to artefactual variation in read density, with more reads being sampled from transcripts and transcript regions whose nucleotide composition is more similar to MNase digestion biases. To verify to what extent our results were affected by this confound, we performed a simulation to determine the expected distribution of reads based on the digestion bias alone (Supplemental Methods). We concluded that MNase biases are unlikely to explain either the enrichment of peaks in exons or the general profile of peak densities past the 3′ splice site.

*d*NET-seq captures recursive splicing intermediates

Having shown that the spliceosome forms a complex with the elongating Pol II in *Drosophila* embryos, we asked when splicing takes place relative to transcription. We first looked at recursive splicing of long introns because this process involves the formation of inherently unstable intermediates that are more likely to be formed soon after the transcription of each intronic splice site (Pai et al. 2018). In recursive splicing, long introns are removed by sequential excision of adjacent sections involving separate splicing reactions, each producing a distinct lariat (Hatton et al. 1998). Recursively spliced intron segments are bounded at one or both ends by recursive sites or ratchet points (Burnette et al. 2005), which correspond to zero nucleotide exons consisting of juxtaposed 3′ and 5′ splice
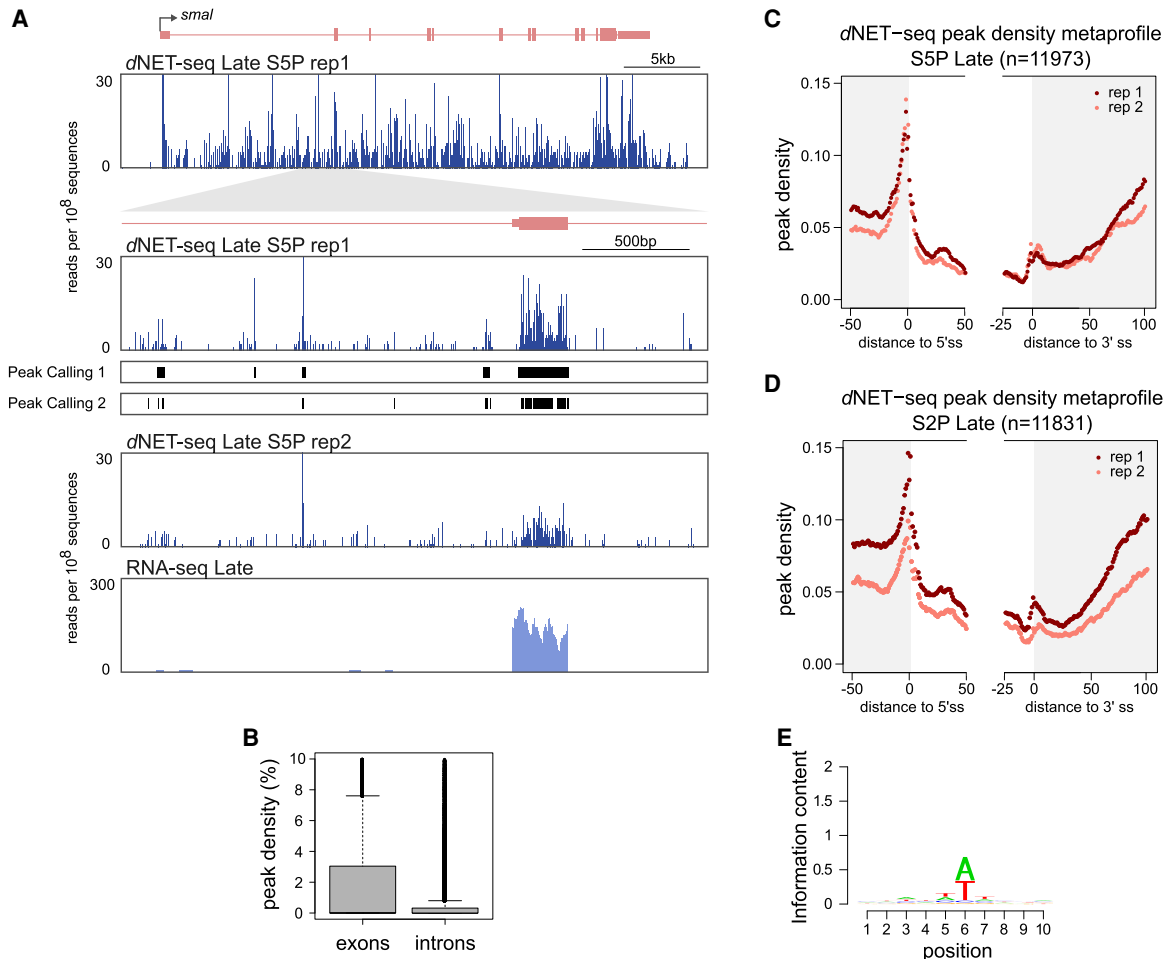
FIGURE 4. Analysis of *d*NET-seq read density profiles. (*A*) *d*NET-seq/S5P and RNA-seq profiles over the post-MBT gene *smoke alarm* (*smal*). The read number is depicted at two magnification levels in two biological replicates. For replicate 1, the line "Peak Caller 1" shows peaks called using the "large peaks" setting, which is appropriate for detecting larger regions of putative Pol II pausing. The line "Peak Caller 2" shows peaks called using the "small peaks" setting, which provides higher spatial resolution and has been used for subsequent analyses. RNA-seq data for the same regions is also shown. (*B*) Peak density in the exons and introns of transcriptionally active genes (*d*NET-seq/S5P, replicate 1). Peak density has been defined as the percentage of nucleotides within a given exon or intron that overlap with a significant peak. (*C,D*) Metagene analysis of peak density estimated from *d*NET-seq/S5P (*C*) and *d*NET-seq/S2P (*D*) data from late embryos. To calculate peak density for each position, we divided the number of introns that overlap with a peak at that position by the total number of introns. The last 50 nt of exons, the first 50 nt of introns, the last 25 nt of introns, and the first 100 nt of exons are shown. Only internal and fully coding exons from transcriptionally active genes that are at least 100 nt long are shown. Exons shorter than 150 nt contribute to both the exon end and start. Only introns that were at least 50 nt long were considered. (*E*) Sequence logo of nucleotide frequencies within a 10-nt window around the 5′ ends of NET-seq reads. The combined height of the bases at each position is proportional to the information content. Position 6 corresponds to the 5′-most nucleotide of the read. Putative internal priming reads, as well as reads mapping to the last nucleotide of exons or introns (possible splice intermediate and intron lariat reads) were ignored.

sites around a central AG|GT motif, where the vertical line represents the splice junction (Fig. 5A).

To capture recursive splicing intermediates using *d*NET-seq, it is essential to have a good coverage of reads corresponding to nascent transcripts and spanning the splice junctions. The total number of reads resulting from nascent RNA in each *d*NET-seq data set is depicted in Supplemental Figure S1G. By merging the sequencing information of overlapped paired-end reads (Fig. 1E), we were able to sequence on average ~103 nt per nascent RNA (Supplemental Fig. S1F,H). Focusing on previously identified *Drosophila* ratchet points (Duff et al. 2015;

Joseph et al. 2018), we found *d*NET-seq/S5P reads that span the junction between the canonical 5′ splice site at the end of the exon and the first ratchet point (RP1) internal to the downstream intron, as shown for the second intron of the *Megalin* gene (Fig. 5B). Reads spanning the subsequent intronic RPs were also observed (Fig. 5B). Overall, we detected *d*NET-seq/S5P and *d*NET-seq/S2P spliced reads supporting most of the previously identified recursive splicing events (Fig. 5C; Supplemental Fig. S5A).

Analysis of *d*NET-seq profiles around a RP reveals an enrichment of reads in a region located a few nucleotides
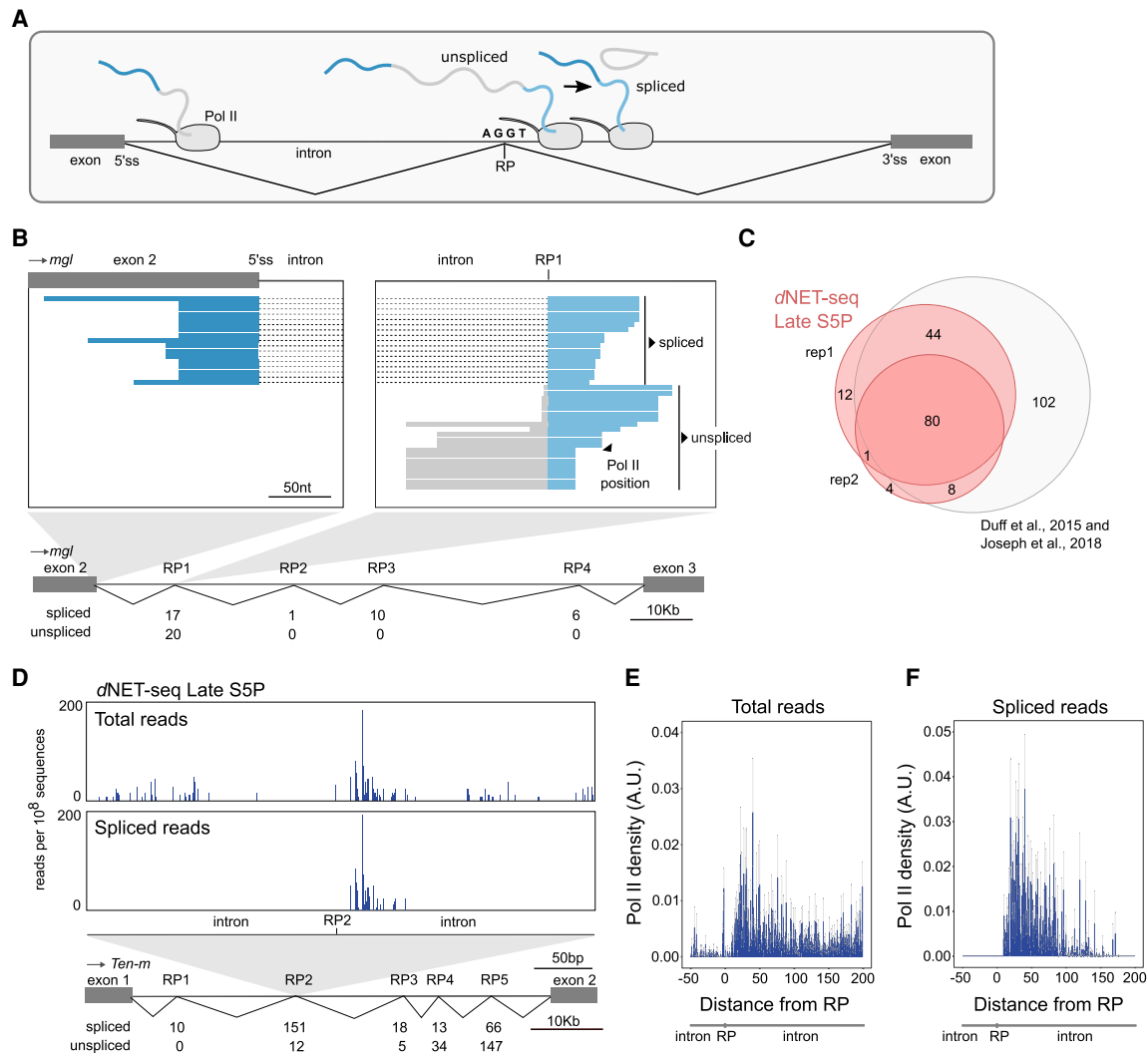
FIGURE 5. *d*NET-seq captures recursive splicing intermediates. (*A*) Schematic illustrating recursive splicing. A ratchet point (RP) with juxtaposed acceptor and donor splice site motifs is indicated. (*B*) Visualization of *d*NET-seq/S5P reads that align to the second intron of the *Megalin* (*mgl*) gene. Recursively spliced reads align to exon 2 (dark blue) and the intron after RP1 (light blue). Unspliced reads are depicted in gray. The number of spliced and unspliced reads at each RP in the intron is indicated. (*C*) Venn diagram comparing RPs identified in two *d*NET-seq/S5P biological replicates and in previously reported studies (Duff et al. 2015; Joseph et al. 2018). (*D*) Number of *d*NET-seq/S5P reads that have the 3′ end mapped around RP2 in the first intron of *Tenascin major* (*Ten-m*) gene. The *top* panel depicts all reads, and the *bottom* panel depicts only reads that have been spliced to RP1. (*E,F*) Meta-analysis with single nucleotide resolution of normalized *d*NET-seq/S5P reads around RPs (*n* = 137) using all reads (*E*) or only reads spliced to the previous RP or exon (*F*).

downstream from the RP, as shown for RP2 in the first intron of the *Tenascin major* gene (Fig. 5D). Noteworthy, most of these reads are already spliced to the previous RP (Fig. 5D). A meta-analysis of *d*NET-seq/S5P reads around 137 RPs confirms that many spliced reads can be observed just downstream from RPs (Fig. 5E,F), demonstrating that splicing occurs soon after the transcription of intronic recursive sites. The observed enrichment of *d*NET-seq/S5P reads around RPs further suggests that recursive splicing and Pol II elongation rate may be kinetically coupled. In agreement with this view, a slow Pol II mutant enhanced recursive splicing of *Ubx* transcripts in *Drosophila* embryos (de la Mata et al. 2003).

Splicing takes place as Pol II transcribes past the 3′ splice site

Having established that *d*NET-seq captures recursive splicing, we then asked whether *d*NET-seq reads spanning canonical exon-exon junctions were also detected (Fig. 6A). To identify splicing events, we considered all internal and fully coding exons that are at least 100 nt long in actively transcribed genes in early and late embryos. For each splice junction, we counted how many reads had the 3′ end mapped to the first 100 nt of the exon. Only exons with at least 10 reads mapping to this region were considered (see the Materials and Methods section for justification of
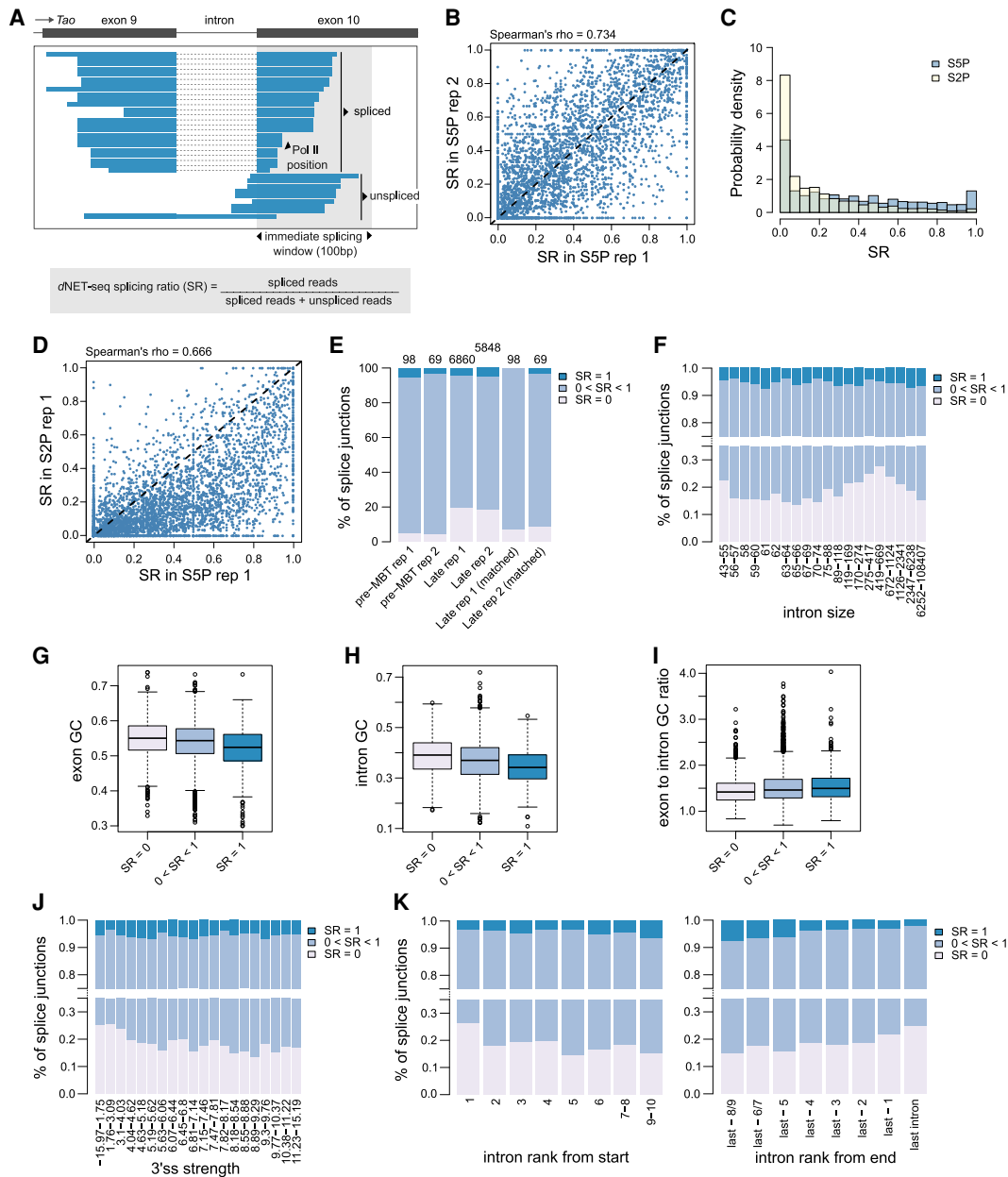
FIGURE 6. dNET-seq reveals immediate splicing at all intron sizes. (A) Visualization of dNET-seq/S5P reads that align to exon 10 of the Tao gene. For B–J, unless otherwise specified, only introns from transcriptionally active genes where the downstream exon is a fully coding internal exon at least 100 nt long were included. In addition, enough spliced/unspliced reads had to end within the first 100 exonic nucleotides that obtaining a splicing ratio (SR) of 0 or 1 by chance alone was highly unlikely (see the Materials and Methods section for details). For genes expressed in late embryos, this threshold was 10 reads for both replicates. For pre-MBT genes, it was 14 for replicate 1 and 9 for replicate 2. For S2P data, we used a threshold of 10 to enable better comparison with S5P. (B) SR values estimated in two biological replicates of dNET-seq/S5P data sets from late embryos (Spearman correlation, $\rho = {\sim}0.734$, $P < 2.2 \times 10^{-16}$; $N = 3708$). (C) Histogram of SR values for dNET-seq/S5P ($N = 5626$) and dNET-seq/S2P ($N = 6888$). To test the significance of the difference between S5P and S2P, a binomial regression with a logit link was performed without filtering by read number ($N = 12{,}833$ for S5P; $N = 13{,}229$ for S2P). The number of spliced and unspliced reads was specified as the dependent variable and the status of each data point as S5P or S2P was the sole predictor. The model predicted a splicing ratio of ${\sim}0.369/{\sim}0.394$ for S5P replicate 1/2 and of $0.162/0.269$ for S2P replicate 1/2. (D) SR values estimated in replicate 1 of dNET-seq/S5P and dNET-seq/S2P data sets from late embryos (Spearman correlation, $\rho = {\sim}0.666$, $P < 2.2 \times 10^{-16}$; $N = 4773$). (E) Proportion of splice junctions in pre-MBT genes and genes expressed in late embryos classified according to their SR values. As many pre-MBT genes are single-intron, last introns were exceptionally included in this analysis. To make the two columns on the right, we used a subset of the genes expressed in late embryos (post-MBT genes) that was as similar as possible to the pre-MBT set in read number. Concretely, to match each pre-MBT gene, we picked the post-MBT gene that had the most similar total count of spliced and unspliced reads, making sure that every post-MBT gene only appeared in the subset once. (F–K) Several parameters of gene architecture show a relationship with SR. For the sample sizes and statistical tests used, see Supplemental Table 1. Note that in F, J–K, the bin ranges have been set so that intron numbers would be as equal as possible between bins.

the threshold). Then, the *d*NET-seq splicing ratio (SR) was calculated by dividing the number of spliced reads by the sum of the number of spliced and unspliced reads (Fig. 6A). Reads could be counted as spliced or unspliced if their 3′ end mapped to within the first 100 nt of the exon and their 5′ end reached upstream of the 3′ splice site, allowing to check whether the intron was still present. A robust agreement of estimated SR values was observed between biological replicates for pre-MBT genes (Supplemental Fig. S6A) and genes expressed in late embryos (Fig. 6B).

SR values showed a bimodal distribution, with peaks at both extremes (SR = 0 and SR = 1; Fig. 6C; Supplemental Fig. S6B), indicating that a subset of junctions were always spliced immediately after transcription (SR = 1), while others remained unspliced (SR = 0). Notably, differences in SR distribution were found between *d*NET-seq/S5P and *d*NET-seq/S2P data sets (Fig. 6C,D; Supplemental Fig. S6B,C). Significantly lower SR values were detected for S2P compared to S5P ($P < 2.2 \times 10^{-16}$ from binomial regression, see Fig. 6 legend for statistical details). In particular, junctions that were most frequently spliced (SR values close to 1) were predominantly captured by *d*NET-seq/S5P (Fig. 6C; Supplemental Fig. S6B). This clearly points to a preferential association between cotranscriptional splicing and S5 phosphorylation of Pol II CTD, as previously proposed in human cells (Nojima et al. 2015, 2018). We therefore continued to focus solely on the S5P data sets in the remainder of our splicing analysis.

We observed that only ~5% of splice junctions in pre-MBT genes were devoid of S5P reads spanning ligated exons and thus presented an SR of 0 (~5.10% replicate 1/ ~4.35% replicate 2), whereas in genes expressed in late embryos this proportion was ~20% (~19.72% replicate 1/ ~18.55% replicate 2) (Fig. 6E; two-tailed binomial test for difference between late and pre-MBT, $P \sim 6.141 \times 10^{-5}$/ 9.44×10^{-4} [replicate 1/replicate 2]). However, this difference between pre-MBT genes and genes expressed in late embryos disappeared once the higher read density of pre-MBT genes had been controlled for (Fig. 6E).

Thus, in most cases, *Drosophila* cotranscriptional splicing can occur when Pol II is still transcribing the downstream exon, implying an intron definition mechanism as previously proposed for *S. cerevisiae* (Carrillo Oesterreich et al. 2016). Consistent with this view, many *Drosophila* transcripts have relatively long exons separated by short introns—a gene architecture suggested to be conducive to intron definition. Very long introns flanked by short exons have instead been associated with exon definition (under which the downstream exon needs to be fully transcribed before splicing can take place) (Keren et al. 2010). A switch to exon definition was proposed once the size of the intron surpasses ~200 nt (Fox-Walsh et al. 2005). It is unclear, however, whether the choice between exon and intron definition is depen-

dent on the absolute sizes of exons and introns, or rather the ratio of intron to exon size.

We found no relationship between the *d*NET-seq splicing ratio and exon length (Supplemental Fig. S6D,H for replicates 1 and 2; see Supplemental Table 1 for details on statistical significance and sample sizes for all of the gene architecture parameters discussed here). Regarding intron size, we found that introns with SR = 0 (and thus no evidence for intron definition) were, on average, indeed larger than other introns (Fig. 6F; Supplemental Fig. S6G). However, more careful examination revealed a more complex picture, with a lower proportion of introns with SR = 0 both for introns of intermediate size (~55–100 nt, which corresponds to ~55% of the introns studied) and for very large introns (>1000 nt) (Fig. 6F). These intron sizes may thus be optimal for fast splicing. We also uncovered a lower exon to intron length ratio for introns with SR = 0 than for others (Supplemental Fig. S6E,I; note that the difference was significant for replicate 2 and near-significant for replicate 1).

Taken together, these results suggest that although fast splicing (implying intron definition) is indeed skewed toward small introns flanked by large exons, there is also frequent and efficient intron definition for large introns. Our results are inconsistent with a threshold model, where splicing would systematically switch to exon definition after a given intron size is reached.

We also investigated the relationship between SR and several other gene architecture parameters. Firstly, as the GC content in exons and introns decreases, the proportion of introns with SR = 1 increases and the proportion with SR = 0 decreases, showing more efficient immediate splicing (Fig. 6G,H; Supplemental Fig. S6K,L). A similar effect is observed as the ratio of the downstream exon GC content to intron GC content increases (Fig. 6I; Supplemental Fig. S6M). Thus, the most efficient immediate splicing is observed when the GC content is low in both exons and introns but higher in exons than introns. Secondly, as 3′ splice site strength increases, the proportion of introns with SR = 0 decreases (Fig. 6J; Supplemental Fig. S6N). We found no significant relationship between SR and 5′ splice site strength (Supplemental Fig. S6F,J). However, we replicated previous observations (Khodor et al. 2012) that transcripts with only a single intron tend to be spliced less efficiently than multiintron ones, with a higher proportion of SR = 0 introns (Supplemental Fig. S6O,P). Thirdly, similarly to previous reports (Khodor et al. 2011, 2012; Herzel et al. 2018), we uncovered an effect of exon rank, whereby exons that are more central appear to be spliced more efficiently (Fig. 6K; Supplemental Fig. S6Q).

In conclusion, *d*NET-seq reveals that splicing can occur immediately as Pol II transcribes past the 3′ splice site, yet many nascent transcripts remain unspliced. As expected, we found a relationship between the proportion of

spliced reads and intron size. However, immediate splicing was observed at all intron sizes.

Immediate splicing associates with specific read density profiles

Analysis of individual *d*NET-seq/S5P profiles around constitutive splice junctions with a high splicing ratio frequently revealed an enrichment of reads downstream from the 3′ splice site, coincident with the appearance of spliced reads, as shown for the *cno* gene (Fig. 7A). In contrast, profiles around a constitutive splice junction with SR = 0 had an accumulation of reads further along the exon, as shown for the *ND-51* gene (Fig. 7B). A clearly distinct type of profile was observed on skipped exons, on which very few reads were observed, as shown for the *zip* gene (Fig. 7C).

We next performed a meta-analysis of *d*NET-seq/S5P peak densities over different exonic and intronic regions for introns with differing SR values. A difficulty of analyzing the peak density profile around the 3′ splice site is that reads mapping to the final nucleotide of the intron may represent intron lariats and thus be nonnascent. We removed reads mapping to this position prior to peak calling. However, through misalignment, intron lariat reads may also map to the few nucleotides around the 3′ splice site and thus still affect the final meta-profile. In order to minimize the impact of such misalignment events, we excluded from the meta-analysis all introns with a read mapping to the final intronic nucleotide, as this is expected to also discard the introns most likely to contain misaligned intron lariat reads (Fig. 7D; Supplemental Fig. S7A). When such filtering is not done, a sharp peak is observed around the 3′ splice site, notably when SR values are low (Supplemental Fig. S7B,C). It appears that intron lariat reads are primarily captured for introns with low splicing ratios (Fig. 7E; Supplemental Fig. S7D). This contrasts with splicing intermediate reads from the end of the upstream exon, which are associated to higher splicing ratios instead (Fig. 7E; Supplemental Fig. S7D).

The peak density profile downstream from the 3′ splice site contains two primary regions of interest (highlighted in Fig. 7D; Supplemental Fig. S7A–C,G,H). The first is a region of increased peak density located roughly 10–20 nt after the 3′ splice site. This peak is independent of the presence of putative intron lariat reads (Fig. 7D; Supplemental Fig. S7A–C), and is more prominent when the SR is higher (Fig. 7D; Supplemental Fig S7A–C,G,H).

The second feature of interest is a rapid increase in peak density ∼60 nt into the exon. Contrary to the first region of interest, the peak density in this region is higher when SR is *lower* (Fig. 7D; Supplemental Fig. S7A–C,G–H). We found no evidence that this increase in peak density could be a result of MNase digestion biases (Supplemental Methods). As discussed above, this pattern of increased *d*NET-seq/S5P density could result from either a local en-

richment of CTD S5 phosphorylation or from an accumulation of Pol II due to a decreased elongation rate. In the latter case, one possible explanation for such a slow-down over exonic regions could be their relatively higher GC content when compared to intronic sequences. The peak is indeed more prominent in introns where the ratio of exonic to intronic GC content is higher (Supplemental Fig. S7E,F). However, when SR = 1, then even exons where this ratio is high do not display the peak (Supplemental Fig. S7E,F). Moreover, introns with higher SR tend to have *higher* exonic to intronic GC ratios (Fig. 6I; Supplemental Fig. S6M). Hence, the covariation with SR cannot be explained simply through the correlation between SR and GC content patterns. This suggests that there is an effect of the SR beyond any GC content effect. Potentially, this region could correspond to where delayed splicing starts (because these events have low immediate splicing ratios). Note that we obtained qualitatively similar meta-profiles when considering read rather than peak densities (Supplemental Fig. S7G,H). Our results therefore cannot be explained through any biases introduced by the peak calling approach.

Finally, we asked how prevalent cotranscriptional splicing is in the developing *Drosophila* embryo. As shown in Figure 2E, ∼80% of exons in pre-MBT genes and genes expressed in late embryos covered by a high density of NET-seq reads have a peak corresponding to the splicing intermediate formed after cleavage at the 5′ splice site but before exon-exon ligation. The majority of these exons (∼85%) were covered by *d*NET-seq reads that span the junction to the downstream exon either directly on nascent transcripts or indirectly on splicing intermediates formed by cleavage at the 5′ splice site of the downstream exon (Fig. 7F,H), confirming that they are cotranscriptionally spliced. We then focused on those exons for which no splicing intermediate spike was detected by the peak calling algorithm, as illustrated for the *Doc3* gene (Fig. 7G). Over 71% of these exons were also covered by *d*NET-seq reads that span the junction to the downstream exon either directly on nascent transcripts or indirectly on splicing intermediates formed by cleavage at the 5′ splice site of the downstream exon (Fig. 7I), arguing that even exons without a detectable splicing intermediate peak are cotranscriptionally spliced. Altogether, our *d*NET-seq results support cotranscriptional splicing for over 95% of the analyzed exons.

DISCUSSION

In this study, we used NET-seq to map Pol II with the CTD phosphorylated on either S5 or S2 positions over the bodies of genes that become transcriptionally active in *Drosophila* embryos during the initial stages of development. The use of embryos allowed us to perform an important test to verify that the captured RNA is truly nascent.
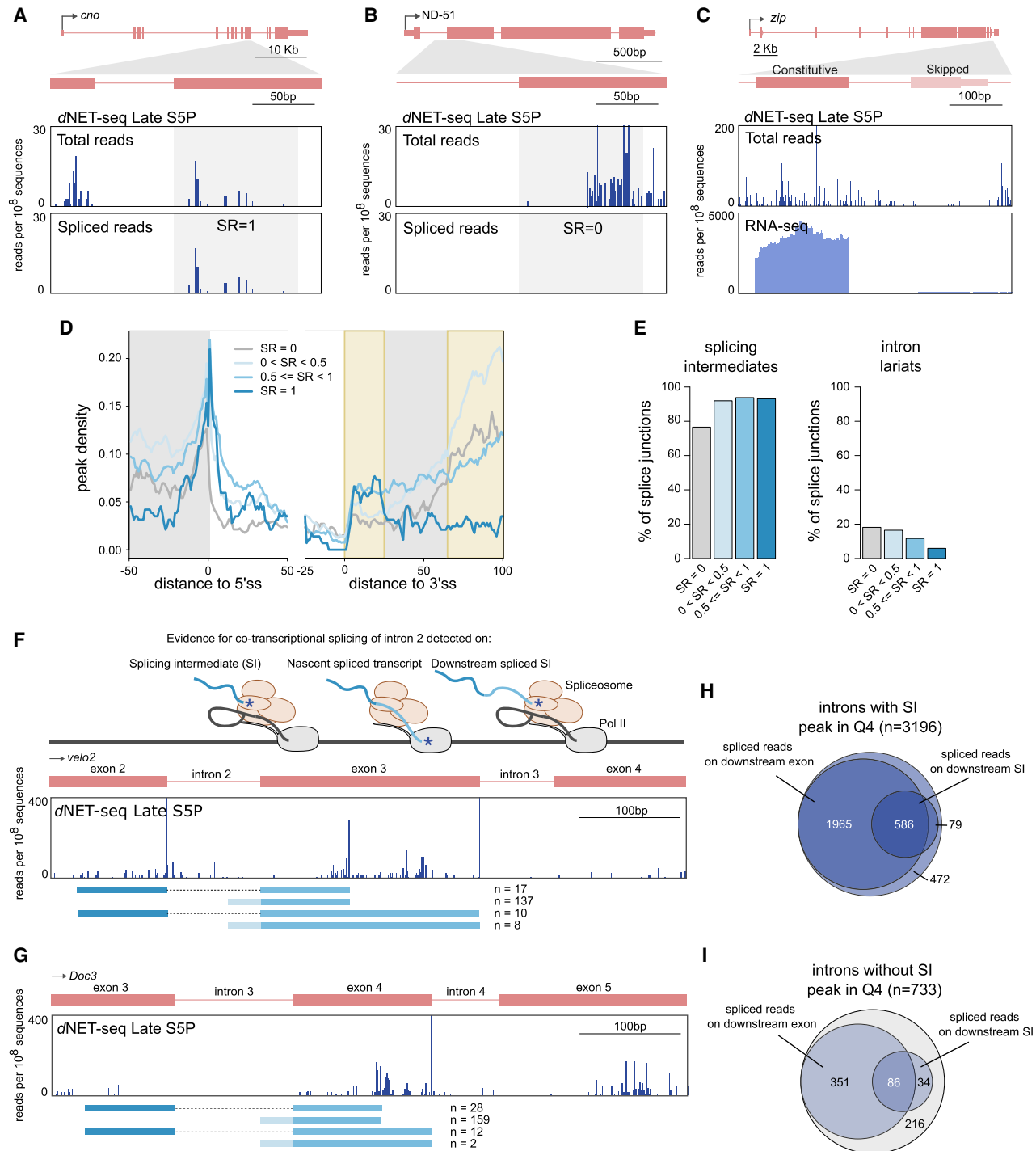
FIGURE 7. Immediate splicing associates with higher density of *d*NET-seq signal. (*A–C*) *d*NET-seq/S5P profiles surrounding the indicated exons in the post-MBT genes *cno* (*A*), *ND-51* (*B*), and *zip* (*C*). The *top* panels depict all reads. The *bottom* panels depict either the 3′ end coordinate of reads that span the splice junction (*A,B*), or the RNA-seq profile (*C*). (*D*) Metagene analysis of peak density estimated from *d*NET-seq/S5P data sets from late embryos (replicate 1) for different ranges of SR values. To calculate peak density for each position, we divided the number of introns that overlap with a peak at that position by the total number of introns. The last 50 nt of exons, the first 50 nt of introns, the last 25 nt of introns, and the first 100 nt of exons are shown. Only internal and fully coding exons from transcriptionally active genes that are at least 100 nt long are shown (*N* = 4783). In addition, at least 10 spliced/unspliced reads had to end within the first 100 nt of the exon. (*E*) The proportion of introns with at least one read whose 3′ end maps to the final position of the upstream exon (putative splicing intermediates) or to the final position of the intron (putative intron lariats) in *d*NET-seq/S5P late replicate 1. (*F,G*) *d*NET-seq/S5P profiles on the indicated regions of the *velo2* and *Doc3* genes. *Below*, spliced reads are depicted. Asterisks denote 3′ OH ends. (*H,I*) Venn diagrams showing how many junctions with or without a splicing intermediate peak are covered by spliced reads or have a downstream splicing intermediate covered by spliced reads.

Indeed, early *Drosophila* embryos contain abundant mRNAs that are transcribed during oogenesis and loaded into the egg. In our analysis of early embryos, these maternal transcripts were readily detected by RNA-seq, but not by *d*NET-seq.

Transcription in the *Drosophila* early embryo begins in mitotic cycle 8 for a few genes (Erickson and Cline 1993; Pritchard and Schubiger 1996), and then the number of active genes gradually increases until cycle 14 (Kwasnieski et al. 2019). Notably, the initial mitotic cycles have a duration of ~10 min, with cycle 13 taking about 21 min and cycle 14 lasting for at least 65 min (Ji et al. 2004). Thus, assuming an elongation rate of 2.4–3.0 kb per minute (Fukaya et al. 2017), there are significant constraints on the transcription of genes that are active before the end of cycle 13 (pre-MBT genes). Although pre-MBT genes are on average shorter than genes expressed at later stages of development (Hoskins et al. 2011; Artieri and Fraser 2014), longer genes are nevertheless transcribed before MBT. However, before cycle 14, transcriptional elongation of long genes is either prematurely terminated (Sandler et al. 2018) or aborted (Shermoen and O'Farrell 1991; Kwasnieski et al. 2019). It has also been reported that pre-MBT expression is associated with the generation of DNA damage due to stalling of DNA replication at transcriptionally engaged loci (Blythe and Wieschaus 2015).

Our *d*NET-seq analysis revealed a novel feature of pre-MBT genes that most likely contributes to reduce conflicts between transcription and replication during the short interphases of early embryos. We found that in the majority of pre-MBT genes, the *d*NET-seq/S5P signal is not detected beyond the pA site, suggesting that Pol II terminates soon after cleavage and polyadenylation. We also observed that these pre-MBT genes tend to be isolated from other transcriptional units. However, a small subset of pre-MBT genes have neighboring genes and in those cases the *d*NET-seq/S5P signal extends past the pA site. In contrast to pre-MBT genes, many of the genes expressed after MBT have the 3′UTR overlapped by another gene transcribed in the opposite direction and show high *d*NET-seq/S5P and S2P signal past the pA site. The finding that very low *d*NET-seq/S5P and S2P signal is detected at the pA site and increases sharply thereafter suggests that nascent transcripts are efficiently cleaved and polyadenylated, yet Pol II remains associated with the DNA template synthesizing RNA past the pA site. Indeed, analysis of RNA-seq data sets confirmed that mRNAs transcribed from these late genes are normally 3′-end processed. Altogether, these observations suggest that transcription termination of isolated genes occurs soon after cleavage and polyadenylation, whereas in genes with overlapping neighbors Pol II continues to transcribe into the gene 3′-flanking region after passage of the pA site. Notably, the proportion of isolated genes is significantly higher among pre-MBT genes (65/117 or ~56%) than among late genes

(1251/7233 or ~17% of all transcriptionally active genes for replicate 1 S5P) ($P < 2.2 \times 10^{-16}$, one-tailed binomial test). Possibly, pre-MBT genes in the *Drosophila* genome may be under selection to avoid overlaps with other genes, thereby minimizing potential transcriptional interference problems such as collisions involving DNA polymerase complexes or Pol II transcribing opposite template strands (Proudfoot 2016).

Our observations further reveal an unexpected link between delayed transcriptional termination and the presence of an overlapping convergent gene in the *Drosophila* genome. It is intriguing that Pol II persists transcribing after cleavage and polyadenylation of the nascent mRNA, specifically when there is a convergent overlapping gene and regardless of its transcriptional status. One possibility is the induction of local conformational changes in chromatin and/or Pol II. Indeed, pioneer transcription factors can potentially regulate gene expression at later stages of development by inducing significant chromatin conformational changes during early embryonic development (Schulz et al. 2015; Blythe and Wieschaus 2016). Although such chromatin remodelling events can potentially influence the interaction of Pol II with DNA downstream from the pA site, further studies are needed to understand how transcription termination is regulated during early *Drosophila* development.

A classical view in the splicing field is that for some introns, the 5′ and 3′ splice sites are recognized directly by "intron definition." For other introns, spliceosome assembly starts with the recognition of the downstream exon, and only at a later stage a cross-intron complex is formed ("exon definition") (Robberson et al. 1990; Berget 1995; Sterner et al. 1996; Fox-Walsh et al. 2005). These alternative models are supported by in vitro evidence, as well as by in vivo reporter gene experiments (Robberson et al. 1990; Berget 1995; Fox-Walsh et al. 2005; De Conti et al. 2013). There is also indirect evidence, for example from analysis of exon-intron size patterns (Berget 1995). However, these models have never been directly tested in vivo at a transcriptome-wide level. It thus remains uncertain how intron definition and exon definition operate in vivo and what determines the choice between them.

Introns that show splicing completion before Pol II has reached the end of the downstream exon are necessarily intron-defined, as exon definition requires the presence of the 5′ splice site of the downstream intron. Therefore, introns with an SR above 0 represent an experimentally determined set of introns that are spliced *via* intron definition at least part of the time, allowing us to test long-held assumptions in the field. Notably, in vitro and reporter gene work suggested that *Drosophila* uses intron definition for introns smaller than ~200–250 nt and exon definition for larger introns (Fox-Walsh et al. 2005). Other studies have suggested that the crucial factor is not just

intron size, but the relative size of the intron compared to the flanking exons (Sterner et al. 1996).

Using *d*NET-seq, we have found that although there is a relationship between intron size and the proportion of introns with SR > 0, intron definition can be observed at all intron sizes. Our results are thus inconsistent with a simple "threshold" model, where splicing would systematically switch to exon definition at a particular intron size. Rather, we observe an increased proportion of introns with SR > 0 within an optimal intron size range of ∼55–100 nt. The median intron size in our data set is 71 nt. It thus appears that intron definition is best optimized for introns of a "typical" size, and is less efficient when introns are unusually small or large. Intriguingly, however, for very large introns (>1000 nt), the proportion with SR > 0 increases again, suggesting that specific mechanisms may have evolved for the intron-defined splicing of very large introns. The tendency for faster splicing kinetics with average intron sizes has also been reported using metabolic labeling in both *Drosophila* (Pai et al. 2017) and human cells (Windhager et al. 2012).

We propose that the tethering of the upstream exon to Pol II (de Almeida and Carmo-Fonseca 2008) could be crucial for the intron-defined splicing of such large introns. Indeed, introns with SR > 0 where the upstream exon has one or more putative splicing intermediate reads tend to be larger than ones without splicing intermediate reads (one-tailed Mann–Whitney *U*-test, W = 779,623, P ∼ 0.003, N = 4589; exon size and read number filtering has been applied like for the gene architecture analysis).

In addition, Pai et al. (2017) found that GC poorer introns were spliced faster. We uncovered a similar relationship with GC content, with the highest proportion of introns with SR > 0 observed when both the exon and the intron were AT-rich but the exon had a higher GC content than the intron. We emphasize that the gene architecture parameters that we have investigated are not independent of each-other. For instance, exon GC content is correlated negatively with exon rank from the start (Spearman's ρ ∼ −0.098; P ∼ 1.196 × 10^{−12}). Further work is thus needed to distinguish between causative and merely correlative factors. In addition, it must be determined how the GC content effect relates to patterns of nucleosome density (Gelfman et al. 2013).

Our results indicate that the majority (>80%) of *Drosophila* introns expressed in late embryos can be spliced through intron definition. A limitation of our work is that introns that show no evidence for splicing completion during transcription of the downstream exon could still be spliced *via* intron definition, if their splicing takes too long for it to be detected during the 100 nt window studied. Therefore, we do not know whether introns with a SR of 0 are exon-defined, intron-defined but spliced when Pol II has elongated past the first 100 exonic nucleotides, or a mixture of both. Similarly, introns with a splicing ratio between 0 and 1 could either always be intron-defined, or they could use either exon or intron definition depending on the splicing event.

Taken together, our results show that splicing in *Drosophila* embryos can be completed soon after transcription of the 3′ splice site, as previously reported in other cellular models (Martin et al. 2013; Carrillo Oesterreich et al. 2016; Reimer et al. 2021; Sousa-Luís et al. 2021). However, a question that remains open is whether splicing influences the kinetics of Pol II elongation. A splicing-dependent Pol II pausing near the 3′ splice site was first suggested by the Beggs group (Alexander et al. 2010; Chathoth et al. 2014), and evidence for Pol II pausing at exon boundaries was later detected in mammalian cells using NET-seq (Mayer et al. 2015; Nojima et al. 2015). In contrast, a recent PRO-seq analysis found no splicing-associated Pol II pausing (Reimer et al. 2021). A splicing-related accumulation of S5P Pol II along gene bodies was also observed using chromatin immunoprecipitation in HeLa cells (Batsché et al. 2006) and in yeast (Alexander et al. 2010; Chathoth et al. 2014). However, it remains unclear whether a local increase in NET-seq read density results from slower Pol II elongation or represents a region of preferential CTD Ser5 phosphorylation, with no concomitant Pol II pausing. In this regard, splicing-associated higher NET-seq density profiles were observed with S5P antibodies but not with antibodies to unphosphorylated CTD (Nojima et al. 2015; Sheridan et al. 2019). Clearly, future studies are needed to assess the distribution of nascent transcripts independently from the Pol II phosphorylation status.

Irrespective of Pol II pausing, the results of our *d*NET-seq/S5P read density analysis around canonical and recursive splice sites strongly suggest that CTD serine 5 can be dynamically rephosphorylated along gene bodies in a splicing-dependent manner, as previously proposed (Harlen and Churchman 2017; Nojima et al. 2018). Moreover, our analysis of nascent *Drosophila* transcripts associated with Pol II S5P CTD revealed highly heterogeneous splicing dynamics. Indeed, while only a minority of splice junctions were devoid of reads spanning ligated exons (corresponding to an SR of 0), many introns remained unspliced in our analysis. In agreement with these observations, a recent single-molecule study of nascent RNA dynamics in live cells found large kinetic variation in intron removal for single introns in single cells (Wan et al. 2021). Is it relevant for cells whether any particular intron is rapidly excised after Pol II transcribes the 3′ splice site or is left unspliced while the transcript elongates? Is the decision to be rapidly excised or left unspliced dependent on a stochastic process? What are the consequences for gene expression of fast versus delayed splicing? Addressing these questions will likely depend on further advances in methodologies to study splicing in time and space at a transcriptome-wide level.

MATERIALS AND METHODS

Embryo collection

Drosophila melanogaster flies (Oregon R [OrR] strain) were raised at 25°C, in polypropylene vials containing standard enriched culture medium (cornmeal, molasses, yeast, soya flour, and beetroot syrup). Three-day-old flies (counting from pupae eclosion) were fattened in culture medium supplemented with fresh yeast for 2 d. Embryos were collected into apple juice-agar plates supplemented with fresh yeast using appropriate cages containing ~200 flies each. To avoid female retention of older embryos, three precollections of 30 min each were made before the first collection of embryos. To maximize egg laying, and avoid larvae contamination, adult flies were transferred to clean embryo collection cages every day over 5 d. For early stage embryos (2–3 h after egg-laying), adult females were allowed to lay eggs for 1 h in apple juice-agar plates. Plates were subsequently collected and embryos were aged at 25°C for 90 min. During the following 30 min, embryos were harvested from the plates, dechorionated in 50% bleach solution for 2 min, and washed once in Phosphate Buffered Saline supplemented with 0.1% Tween-20 (PBT) and twice in deionized water. In order to discard older embryos (stage 6 and older), manual staging of collected embryos was performed with the help of forceps and under a magnifier scope. Embryos were then resuspended in a solution containing 120 mM NaCl and 0.04% Triton, and washed twice with 120 mM NaCl solution. At the end of the 3 h collection, the solution was removed and embryos were frozen in liquid nitrogen and stored at −80°C. For the late stage (4–6 h), eggs were laid for 2 h and aged at 25°C for 3.5 h. Embryo collection and processing was similar to the early stage embryos, but in this case, no manual staging was performed.

Embryo DNA staining

For each embryo collection, and after dechorionation, a representative embryo sample was collected from the total pool and fixed in a scintillation flask, using a solution containing one volume of 4% formaldehyde in PBT and four volumes of heptane, for 20 min at 100 rpm. The lower aqueous phase solution was subsequently removed, 4 mL of methanol was added and embryos were shaken vigorously for 1 min. Embryos were then collected from the bottom of the scintillation flask, washed twice with methanol, and frozen at −20°C in methanol. To rehydrate the embryos, they were washed for 5 min each, with 3:1, 1:1, and 1:3 mix solutions of methanol:PBT. Embryos were subsequently washed twice in PBT and incubated with 1:5000 Sytox green (Invitrogen), supplemented with 5 µg/mL RNase A (Sigma-Aldrich) in PBT for 15 min. After washing with PBT, embryos were mounted in fluorescence mounting medium (Dako) and examined in a Zeiss AxioZoom V16 Fluorescence Stereo Microscope for image acquisition and embryo staging. Images were processed using ImageJ software (NIH).

*d*NET-seq and library preparation

The *d*NET-seq protocol was adapted from mNET-seq (Nojima et al. 2016). Briefly, 300 µL of frozen embryos was resuspended in 3.5 mL of Buffer B1 (15 mM HEPES-KOH, pH 7.6; 10 mM KCl; 5 mM $MgCl_2$; 1 mM DTT; 0.1 mM EDTA; 0.35 M sucrose; 4 µg/mL pepstatin; 10 mM sodium netabisulfite; 0.5 mM EGTA supplemented with complete EDTA free protease inhibitor [Roche] and PhoSTOP [Roche]). Embryos were homogenized in a Dounce homogenizer with 11× strokes using a tight pestle on ice. The suspension was centrifuged at 7700g for 15 min at 4°C, the supernatant was discarded, and the white pellet containing the nuclei was resuspended in 500 µL of Buffer B1. The suspension was again homogenized in the Dounce with 4× strokes and loaded without mixing on the top of buffer B2 (15 mM HEPES-KOH, pH 7.6; 10 mM KCl; 5 mM $MgCl_2$; 1 mM DTT; 0.1 mM EDTA; 0.8 M sucrose; 4 µg/mL pepstatin; 10 mM sodium metabisulfite; 0.5 mM EGTA supplemented with complete EDTA free protease inhibitor [Roche] and PhosSTOP [Roche]). The suspension was centrifuged at 1310g for 30 min at 4°C, and the pellet was resuspended with 125 µL of NUN1 buffer (20 mM Tris-HCl [pH 7.9]; 75 mM NaCl; 0.5 mM EDTA and 50% Glycerol). An amount of 1.2 mL of Buffer NUN2 (300 mM NaCl, 7.5 mM $MgCl_2$, 1% NP-40, 1 M Urea supplemented with complete EDTA free protease inhibitor [Roche] and PhoSTOP [Roche]) was mixed with the nuclei and incubated on ice for 15 min performing a short vortex every 3 min. Chromatin was then centrifuged at 10,000g for 10 min at 4°C, washed with 100 µL of 1× MNase Buffer, and incubated in 100 µL of MNase reaction mixing (1× MNase buffer and 30 gel unit/µL MNase [New England Biolabs]) for 3 min at 37°C with mixing at 1400 rpm. The reaction was stopped with 10 µL of 250 mM EGTA, centrifuged at 10,000g for 5 min at 4°C, and the supernatant containing the solubilized chromatin was recovered. For the early embryos sample, 2 × 300 µL of embryos were prepared in parallel and pooled together after the chromatin solubilization. Immunoprecipitation of Pol II–RNA complexes was performed using 50 µL of Protein G Dynabeads (Thermo Fisher Scientific), preincubated overnight with 5 µg of the correspondent antibody: anti-Pol II CTD S5P (ab5131 Abcam) or anti-Pol II CTD S2P (ab5095 Abcam) in 100 µL NET2 (50 mM Tris-HCl pH 7.4; 150 mM NaCl and 0.05% NP-40) and washed three times with NET2. Beads were incubated with the solubilized chromatin in 1 mL total volume of NET2 for 1 h at 4°C, washed seven times with 500 µL of NET2 and once with 100 µL of PNKT (1× PNK buffer and 0.1% tween) before incubation for 6 min in 50 µL of PNK reaction mix (1× PNKT, 1 mM ATP and 0.05 U/mL T4 PNK 3'phosphatase minus [NEB] in a thermomixer at 37°C and 1400 rpm. After washing the beads with NET2, long RNA fragments were isolated using Quick-RNA MicroPrep (Zymo research): 300 µL of RNA Lysis Buffer in 33% EtOH was mixed to the beads by pipetting. Beads were discarded and the suspension was loaded into a Zymo spin column that was centrifuged at 10,000g for 30 sec. The column was washed once with 400 µL RNA prep buffer and twice with 700 µL and 400 µL RNA wash buffer, respectively. RNA was then eluted in 15 µL of DNase/RNase-free water (Zymo) and stored at −80°C. An amount of 100 ng of RNA was used to prepare each library, following the standard protocol of the TruSeq Small RNA Library Prep kit (Illumina). After adapter ligation and reverse transcription, the libraries were PCR amplified using 16 PCR cycles, and cDNA libraries were fractionated in the gel between 130 to 300 bp. The libraries were sequenced using PE-150 on the Illumina HiSeq X platform by Novogene Co., Ltd.

Quantification and statistical analysis

dNET-seq data processing

Adapter sequences were removed from all *d*NET-seq paired-end samples using Cutadapt (version 1.18) (Martin 2011) with the following parameters: -a TGGAATTCTCGGGTGCCAAGG -A GATCGTCGGACTGTAGAACTCTGAAC -m 10 -e 0.05 –match-read-wildcards -n 1. Paired-end read merging was performed using bbmerge.sh from BBMap (Bushnell et al. 2017) with the "xloose" parameter. Merged reads were then aligned to the *Drosophila* reference genome (*dm6*; Ensembl release 95) (Cunningham et al. 2019) using STAR (version 2.6.0b) (Dobin et al. 2013) with –chimSegmentMin set to 20. Only uniquely mapped reads were considered, extracted using SAMtools (version 1.7) (Li et al. 2009) with -q set to 255. Exceptionally, in Supplemental Figure S2A, HiSat2 was used, using the same dm6 genome annotation file for genome indexing and using default parameters, with the –no-discordant –no-mixed flags set. PCR internal priming events generated during library preparation were removed using a custom Python script (Prudêncio et al. 2020) with the following parameters: -a TGG.. -s paired. To obtain single-nucleotide resolution, a custom Python script (Prudêncio et al. 2020) was used to extract the 5′ end nucleotide of read 2 (after trimming) in each sequencing pair, with the directionality indicated by read 1 (Fig. 1E).

Publicly available RNA-seq data sets used

Publicly available *Drosophila* embryonic transcriptome sequencing data [Poly(A) RNA-seq], performed in developmental stages similar to the dNET-seq early and late samples, were used in this study. RNA-seq data sets corresponding to cycle 14B (Lott et al. 2011) were obtained from the Gene Expression Omnibus (GEO) (samples GSM618409, GSM618410, GSM618421, and GSM618422 from data set GSE25180). RNA-seq data sets from 4–6 h old embryos were obtained from modENCODE project PRJNA75285 (Graveley et al. 2011) (accessions SRR023696, SRR023746, SRR023836, SRR035220, SRR023669, SRR035405, SRR035406, SRR024014, and SRR023539).

RNA-seq data processing

Adapters were removed from all data sets using Trim Galore (version 0.4.4) (http://www.bioinformatics.babraham.ac.uk/projects/trim_galore/; last accessed 26 April 2020). Data sets from modENCODE and GEO were aligned to the *dm6 Drosophila* reference genome (Ensembl release 95) (Cunningham et al. 2019) using STAR (version 2.6.0b) (Dobin et al. 2013) with –chimSegmentMin set to 20. Stringtie (version 1.3.3b) (Pertea et al. 2015) was used to quantify normalized gene expression as Transcripts Per Kilobase Million (TPM) values with the following parameters: -a 5 -e. In addition, the isoform list was provided together with the -G parameter corresponding to the *dm6* (Ensembl release 95) GTF file. Genes with TPM values above 2 were considered to be expressed.

Selection of genes and isoforms for analysis

Similar to a previous GRO-seq analysis (Core et al. 2008), we used the read density of very large intergenic regions (gene desert re-

gions) to define the reference for absence of transcription. Gene deserts were divided into 50kb windows, and *d*NET-seq read densities were calculated by dividing the read counts in each window by the window length (in bp). Read counts per window were obtained with bedtools genome coverage (version 2.27.1-1-gb87c465) (Quinlan and Hall 2010), and an arbitrary density threshold was defined as the 90th percentile of the read density distribution (Supplemental Fig. S4A). Transcripts whose gene body *d*NETseq read density exceeded this threshold were considered to be transcriptionally active (Supplemental Fig. S4B). For all of the analyses performed on late genes, only transcriptionally active genes were considered. In addition, only one isoform per gene was considered for all analysis, selected as the isoform with the highest RPKM value in the RNA-seq data set for the corresponding developmental stage.

The coordinates of previously identified pre-MBT genes were obtained from Chen et al. (2013) and converted to *dm6* coordinates using the *liftOver* tool (https://genome.ucsc.edu/cgi-bin/hgLiftOver). The most representative isoform for each gene was manually selected through visualization of individual profiles.

Splicing intermediate and lariat detection

Exons containing splicing intermediates or introns containing lariats were identified using a peak finder algorithm (NET_snrPeakFinder) (Churchman and Weissman 2011; Prudêncio et al. 2020) that detects the presence of a peak in the last nucleotide of an exon (splicing intermediate) or an intron (lariat), by comparing the accumulation of 3′ end reads mapping at that position with the mean read density of the flanking 200 nt. A peak is called when the read density at the peak is superior to the mean of this surrounding region plus 3 standard deviations (Churchman and Weissman 2011). Since gene read density influences peak detection, the exons were divided into quartiles based on the *d*NET-seq read density of the corresponding gene. Only exons from the highest quartile (i.e., from genes with the highest read density) were considered in Figure 2 for *d*NET-seq Late analysis.

Analysis of read density and peak calling

RPKM values for the merged *d*NET-seq data sets were calculated in the following manner:

$$\text{RPKM (transcript)} =$$
$$\frac{\text{reads} \times 10^4 \times 10^6}{(\text{total uniquely mapped reads}) \times (\text{gene length in bp})},$$

where 10^4 normalizes for gene length and 10^6 normalizes for sequencing depth. Queries of gene 3′UTR overlaps (Fig. 3) between genes were performed with bedtools intersect (version 2.27.1-1-gb87c465) (Quinlan and Hall 2010).

To detect splicing intermediate and intron lariat peaks, the algorithm from Churchman and Weissman (2011) was adapted as described in Prudêncio et al. (2020). To be able to call larger regions as peaks, a custom algorithm was developed and implemented in Python 3.7. Note that like for all of the custom Python code reported here, there is heavy reliance on *bedtools* v2.29.0 (Quinlan and Hall 2010) for operations on coordinate intervals. In addition, NumPy v1.17.2 (Harris et al. 2020) and SciPy 1.4.0 (Virtanen et al. 2020) were used. Our peak caller detects

regions where the local read density is significantly higher than expected by chance given the overall read density of the transcript. Almost all of the numerical parameters used by the peak caller can be adjusted. In Figure 4A, results obtained with two particular parameterizations are shown. Peak Caller 1 ("large peaks") is adapted to detecting larger peaks and provides results that are more intuitive to a human observer. Peak Caller 2 ("small peaks") provides a finer spatial resolution, and corresponds to the settings used in all of the analyses in this study. The peak caller takes as input a BED file with the 3′ ends of reads (single-nucleotide resolution), as well as a GTF file with transcript and exon annotations and a list of transcripts to analyze. It functions by calculating a sliding average of read density within each transcript (window size 5/21 for small/large; only reads mapping to the same strand as the annotated transcript are considered). It then randomly shuffles the positions of the reads within the transcript and recalculates the sliding averages to determine the random expectation. This can be repeated several times (five in this study) for more robustness. Windows obtained with the true read distribution are called as significant if their read density is higher than the 99th percentile of the simulated windows. Note that in this study, we used a setting whereby this threshold is calculated separately for each exon (and its upstream intron, for exons other than the first), by excluding the intron-exon pair of interest and reads overlapping it during the simulation step. This is necessary so that when calling peaks within a given exon (and its upstream intron), the threshold set would not be affected by the reads within that particular exon and its upstream intron. This way, for instance, the calling of a peak in the beginning of the exon is not affected by the calling of a peak in the middle of the same exon (except through potential merging, see below). After the initial peaks are called, they are filtered to remove peaks where more than 90% of the reads come from a single nucleotide (probable PCR duplicates), that are shorter than 5 nt, or that overlap with fewer reads than a specified threshold (10/5 for large/small). Finally, peaks that are within a specified distance of each-other (21/5 nt for large/small) are merged together.

Individual gene profiles

Individual dNET-seq gene profiles were generated by separating reads by strand using SAMtools (version 1.7) (Li et al. 2009). Strand-separated read data was converted to bedGraph format using bedtools genomecov with the -bg flag (version 2.27.1-1-gb87c465) (Quinlan and Hall 2010). Coverage values were normalized per nucleotide accounting for the total number of uniquely aligned reads and with the scale set to reads per 10^8 sequences. The outcome was converted to bigwig files through the bedGraphToBigWig tool (Kent et al. 2010) and uploaded to the UCSC Genome Browser (James Kent et al. 2002).

Metagene analysis

The read density metagene plots in Figure 3F–I and Figure 5E,F were created with deepTools (version 3.0.2) (Ramírez et al. 2016). Metagenes with normalized gene size (Fig. 3) have bins of 10 bp while all other metagene plots in this study have single nucleotide resolution. Normalized gene and intron lengths (Fig. 3F–I) were obtained through the scale-regions option. Exon-intron junctions without normalized lengths were obtained using

the reference-option set to the 3′SS or the 5′SS. For normalization, we divided the number of reads at each nucleotide (or bin) by the total number of reads in the entire genomic region under analysis. These values were then used to calculate the mean for each nucleotide, and the results were plotted in arbitrary units (A.U.) ranging from 0 to 1.

The peak or read density metagene plots in Figures 3D, 4B and 7D, and Supplemental Figures S3G, S7A–G, and S7E–J were prepared using custom Python and R scripts (https://github.com/rosinaSav/dNETseq_code). The peak density value represents the proportion of introns/exons that overlap with a peak at that position. Only internal fully coding exons that were at least 100 nt long were included. In addition, the intron just upstream of the exon had to be at least 50 nt long. For Figure 7D, Supplemental Figures S7A–G and S7E–H, further filtering based on read coverage was performed (see below). Note that exons shorter than 150 nucleotides contribute both to the upstream and downstream exonic proportion of the plot.

Immediate splicing analysis

The immediate splicing analysis was performed solely on the S5P data sets. Only the 117 previously annotated pre-MBT genes (Chen et al. 2013) were analyzed for early data sets. Reads were considered as spliced if they contained "N"s in the CIGAR string, in a position corresponding to an annotated intron. Reads that overlapped both the (unspliced) intron and the downstream exon were considered as unspliced. In both cases, only reads where the 3′ end was located at least 5 nt downstream from the 3′ ss were included, to avoid analyzing misaligned reads whose 3′ end should have mapped to the end of the upstream exon instead. Spliced reads that had the 5′ end mapped to the upstream exon and the 3′ end mapped to the intron were considered indicative of recursive splicing if the first nucleotide of the downstream end (indicative of the ratchet point position) matched the second G in the AGGT canonical splicing motif. If the last nucleotide of a read matched the last nucleotide of an exon, it was considered a splicing intermediate read and not representative of nascent RNA. A splicing ratio was calculated by dividing the number of nascent RNA spliced reads by the sum of the number of spliced and unspliced nascent RNA reads, only including reads whose 3′ ends mapped to the first 100 nt of the downstream exon. Only fully coding internal exons at least 100 nt long were considered (exceptionally, in Fig. 6E and K and Supplemental Fig. S6O–Q, the 3′ most coding exon was also analyzed). Finally, we performed filtering to remove exons where the read coverage was too low to allow for robust estimation of the splicing ratio. The relevant threshold was calculated for each data set separately. We calculated the total proportion of spliced reads out of all spliced/unspliced reads for the data set to obtain the expected splicing ratio. We then performed a binomial test to know the probability of sampling only spliced/unspliced reads by chance under the null that the true splicing ratio equaled this expectation. We set the threshold as the lowest number of reads that had to be sampled for the probability to be below 0.01. Through this procedure, the threshold was set at ≥10 reads for replicate 1 and 2 of the late data set (no terminal coding exons), at ≥11/10 reads for replicate 1/2 of the late data set including terminal coding exons, and at ≥14/9 reads for replicate 1/2 of the early data set (terminal coding exons always included).

Gene architecture and nucleotide composition analysis

Gene architecture and nucleotide composition parameters were calculated using custom Python and R scripts based on Ensembl annotations for dm6.18 (Cunningham et al. 2019). Splice site strength scores were calculated using MaxEntScan (Yeo and Burge 2004) with default parameters. Significance testing was performed using Kruskal–Wallis tests with a Bonferroni correction for multiple comparisons, with the correction applied separately for either replicate. For predictors where the corrected *P*-value was <0.05, Dunn's test was performed on the pairwise comparisons using *R* package *dunn.test* (Dinno 2017). The sequence logo in Figure 4E was generated using the *seqLogo* package version 1.52.0 in R (Bembom 2019).

DATA DEPOSITION

All raw and processed sequencing data generated in this study have been submitted to the NCBI Gene Expression Omnibus (GEO; https://www.ncbi.nlm.nih.gov/geo/) under accession number GSE152585. The Python code used is available at https://github.com/rosinaSav/dNETseq_code and https://github.com/kennyrebelo.

SUPPLEMENTAL MATERIAL

Supplemental material is available for this article.

ACKNOWLEDGMENTS

REFERENCES

Akhtar J, Kreim N, Marini F, Mohana G, Brüne D, Binder H, Roignant J-Y. 2019. Promoter-proximal pausing mediated by the exon junction complex regulates splicing. *Nat Commun* **10:** 521. doi:10.1038/s41467-019-08381-0

Alexander RD, Innocente SA, Barrass JD, Beggs JD. 2010. Splicing-dependent RNA polymerase pausing in yeast. *Mol Cell* **40:** 582–593. doi:10.1016/j.molcel.2010.11.005

Alpert T, Herzel L, Neugebauer KM. 2017. Perfect timing: splicing and transcription rates in living cells. *WIREs RNA* **8:** e1401. doi:10.1002/wrna.1401

Ameur A, Zaghlool A, Halvardson J, Wetterbom A, Gyllensten U, Cavelier L, Feuk L. 2011. Total RNA sequencing reveals nascent transcription and widespread co-transcriptional splicing in the human brain. *Nat Struct Mol Biol* **18:** 1435–1440. doi:10.1038/nsmb.2143

Artieri CG, Fraser HB. 2014. Transcript length mediates developmental timing of gene expression across *Drosophila. Mol Biol Evol* **31:** 2879–2889. doi:10.1093/molbev/msu226

Arzate-Mejía RG, Josué Cerecedo-Castillo A, Guerrero G, Furlan-Magaril M, Recillas-Targa F. 2020. In situ dissection of domain boundaries affect genome topology and gene transcription in *Drosophila. Nat Commun* **11:** 894. doi:10.1038/s41467-020-14651-z

Aslanzadeh V, Huang Y, Sanguinetti G, Beggs JD. 2018. Transcription rate strongly affects splicing fidelity and cotranscriptionality in budding yeast. *Genome Res* **28:** 203–213. doi:10.1101/gr.225615.117

Batsché E, Yaniv M, Muchardt C. 2006. The human SWI/SNF subunit Brm is a regulator of alternative splicing. *Nat Struct Mol Biol* **13:** 22–29. doi:10.1038/nsmb1030

Bembom O. 2019. *seqLogo: sequence logos for DNA sequence alignments.* R package version 1.52.0.

Berget SM. 1995. Exon recognition in vertebrate splicing. *J Biol Chem* **270:** 2411–2414. doi:10.1074/jbc.270.6.2411

Beyer AL, Osheim YN. 1988. Splice site selection, rate of splicing, and alternative splicing on nascent transcripts. *Genes Dev* **2:** 754–765. doi:10.1101/gad.2.6.754

Blythe SA, Wieschaus EF. 2015. Coordinating cell cycle remodeling with transcriptional activation at the *Drosophila* MBT. *Curr Top Dev Biol* **113:** 113–148. doi: 10.1016/bs.ctdb.2015.06.002

Blythe SA, Wieschaus EF. 2016. Establishment and maintenance of heritable chromatin structure during early *Drosophila* embryogenesis. *Elife* **5:** e20148. doi:10.7554/eLife.20148

Boija A, Mahat DB, Zare A, Holmqvist P-H, Philip P, Meyers DJ, Cole PA, Lis JT, Stenberg P, Mannervik M. 2017. CBP regulates recruitment and release of promoter-proximal RNA polymerase II. *Mol Cell* **68:** 491–503.e5. doi:10.1016/j.molcel.2017.09.031

Brugiolo M, Herzel L, Neugebauer KM. 2013. Counting on co-transcriptional splicing. *F1000Prime Rep* **5:** 9. doi:10.12703/P5-9

Burnette JM, Miyamoto-Sato E, Schaub MA, Conklin J, Lopez AJ. 2005. Subdivision of large introns in *Drosophila* by recursive splicing at nonexonic elements. *Genetics* **170:** 661–674. doi:10.1534/genetics.104.039701

Bushnell B, Rood J, Singer E. 2017. BBMerge: accurate paired shotgun read merging via overlap. *PLoS One* **12:** e0185056. doi:10.1371/journal.pone.0185056

Campos-Ortega JA. 1985. Genetics of early neurogenesis in *Drosophila melanogaster. Trends Neurosci* **8:** 245–250. doi:10.1016/0166-2236(85)90097-9

Carrillo Oesterreich F, Preibisch S, Neugebauer KM. 2010. Global analysis of nascent RNA reveals transcriptional pausing in terminal exons. *Mol Cell* **40:** 571–581. doi:10.1016/j.molcel.2010.11.004

Carrillo Oesterreich F, Herzel L, Straube K, Hujer K, Howard J, Neugebauer KM. 2016. Splicing of nascent RNA coincides with intron exit from RNA polymerase II. *Cell* **165:** 372–381. doi:10.1016/j.cell.2016.02.045

Chathoth KT, Barrass JD, Webb S, Beggs JD. 2014. A splicing-dependent transcriptional checkpoint associated with prespliceosome formation. *Mol Cell* **53:** 779–790. doi:10.1016/j.molcel.2014.01.017

Chen K, Johnston J, Shao W, Meier S, Staber C, Zeitlinger J. 2013. A global change in RNA polymerase II pausing during the

Drosophila midblastula transition. *Elife* **2:** e00861. doi:10.7554/eLife.00861

Churchman LS, Weissman JS. 2011. Nascent transcript sequencing visualizes transcription at nucleotide resolution. *Nature* **469:** 368–373. doi:10.1038/nature09652

Core LJ, Waterfall JJ, Lis JT. 2008. Nascent RNA sequencing reveals widespread pausing and divergent initiation. *Science* **322:** 1845–1849. doi:10.1126/science.1162228

Cunningham F, Achuthan P, Akanni W, Allen J, Amode MR, Armean IM, Bennett R, Bhai J, Billis K, Boddu S, et al. 2019. Ensembl 2019. *Nucleic Acids Res* **47:** D745–D751. doi:10.1093/nar/gky1113

Dahlberg O, Shilkova O, Tang M, Holmqvist P-H, Mannervik M. 2015. P-TEFb, the super elongation complex and mediator regulate a subset of non-paused genes during early *Drosophila* embryo development. *PLoS Genet* **11:** e1004971. doi:10.1371/journal.pgen.1004971

David CJ, Boyne AR, Millhouse SR, Manley JL. 2011. The RNA polymerase II C-terminal domain promotes splicing activation through recruitment of a U2AF65–Prp19 complex. *Genes Dev* **25:** 972–982. doi:10.1101/gad.2038011

de Almeida SF, Carmo-Fonseca M. 2008. The CTD role in cotranscriptional RNA processing and surveillance. *FEBS Lett* **582:** 1971–1976. doi:10.1016/j.febslet.2008.04.019

De Conti L, Baralle M, Buratti E. 2013. Exon and intron definition in pre-mRNA splicing. *Wiley Interdiscip Rev RNA* **4:** 49–60. doi:10.1002/wrna.1140

de la Mata M, Alonso CR, Kadener S, Fededa JP, Blaustein M, Pelisch F, Cramer P, Bentley D, Kornblihtt AR. 2003. A slow RNA polymerase II affects alternative splicing in vivo. *Mol Cell* **12:** 525–532. doi:10.1016/j.molcel.2003.08.001

Dingwall C, Lomonossoff GP, Laskey RA. 1981. High sequence specificity of micrococcal nuclease. *Nucleic Acids Res* **9:** 2659–2674. doi:10.1093/nar/9.12.2659

Dinno A. 2017. dunn.test: Dunn's test of multiple comparisons using rank sums. R package version 1.3.5. https://cran.r-project.org/web/packages/dunn.test/index.html

Dobin A, Davis CA, Schlesinger F, Drenkow J, Zaleski C, Jha S, Batut P, Chaisson M, Gingeras TR. 2013. STAR: ultrafast universal RNA-seq aligner. *Bioinformatics* **29:** 15–21. doi:10.1093/bioinformatics/bts635

Drexler HL, Choquet K, Churchman LS. 2020. Splicing kinetics and coordination revealed by direct nascent RNA sequencing through nanopores. *Mol Cell* **77:** 985–998.e8. doi:10.1016/j.molcel.2019.11.017

Duff MO, Olson S, Wei X, Garrett SC, Osman A, Bolisetty M, Plocik A, Celniker SE, Graveley BR. 2015. Genome-wide identification of zero nucleotide recursive splicing in *Drosophila*. *Nature* **521:** 376–379. doi:10.1038/nature14475

Emili A, Shales M, McCracken S, Xie W, Tucker PW, Kobayashi R, Blencowe BJ, Ingles CJ. 2002. Splicing and transcription-associated proteins PSF and p54^{nrb}/NonO bind to the RNA polymerase II CTD. *RNA* **8:** 1102–1111. doi:10.1017/S1355838202025037

Erickson JW, Cline TW. 1993. A bZIP protein, sisterless-a, collaborates with bHLH transcription factors early in *Drosophila* development to determine sex. *Genes Dev* **7:** 1688–1702. doi:10.1101/gad.7.9.1688

Fong N, Kim H, Zhou Y, Ji X, Qiu J, Saldi T, Diener K, Jones K, Fu XD, Bentley DL. 2014. Pre-mRNA splicing is facilitated by an optimal RNA polymerase II elongation rate. *Genes Dev* **28:** 2663–2676. doi:10.1101/gad.252106.114

Fox-Walsh KL, Dou Y, Lam BJ, Hung SP, Baldi PF, Hertel KJ. 2005. The architecture of pre-mRNAs affects mechanisms of splice-site pairing. *Proc Natl Acad Sci* **102:** 16176–16181. doi:10.1073/pnas.0508489102

Fukaya T, Lim B, Levine M. 2017. Rapid rates of Pol II elongation in the *Drosophila* embryo. *Curr Biol* **27:** 1387–1391. doi:10.1016/j.cub.2017.03.069

Gaffney DJ, McVicker G, Pai AA, Fondufe-Mittendorf YN, Lewellen N, Michelini K, Widom J, Gilad Y, Pritchard JK. 2012. Controls of nucleosome positioning in the human genome. *PLoS Genet* **8:** e1003036. doi:10.1371/journal.pgen.1003036

Gelfman S, Cohen N, Yearim A, Ast G. 2013. DNA-methylation effect on cotranscriptional splicing is dependent on GC architecture of the exon-intron structure. *Genome Res* **23:** 789–799. doi:10.1101/gr.143503.112

Görnemann J, Barrandon C, Hujer K, Rutz B, Rigaut G, Kotovic KM, Faux C, Neugebauer KM, Séraphin B. 2011. Cotranscriptional spliceosome assembly and splicing are independent of the Prp40p WW domain. *RNA* **17:** 2119–2129. doi:10.1261/rna.02646811

Graveley BR, Brooks AN, Carlson JW, Duff MO, Landolin JM, Yang L, Artieri CG, Van Baren MJ, Boley N, Booth BW, et al. 2011. The developmental transcriptome of *Drosophila melanogaster*. *Nature* **471:** 473–479. doi:10.1038/nature09715

Guilgur LG, Prudêncio P, Sobral D, Liszekova D, Rosa A, Martinho RG. 2014. Requirement for highly efficient pre-mRNA splicing during *Drosophila* early embryonic development. *Elife* **3:** e02181. doi:10.7554/eLife.02181

Harlen KM, Churchman LS. 2017. The code and beyond: transcription regulation by the RNA polymerase II carboxy-terminal domain. *Nat Rev Mol Cell Biol* **18:** 263–273. doi:10.1038/nrm.2017.10

Harris CR, Millman KJ, van der Walt SJ, Gommers R, Virtanen P, Cournapeau D, Wieser E, Taylor J, Berg S, Smith NJ, et al. 2020. Array programming with NumPy. *Nature* **585:** 357–362. doi:10.1038/s41586-020-2649-2

Hatton AR, Subramaniam V, Lopez AJ. 1998. Generation of alternative *Ultrabithorax* isoforms and stepwise removal of a large intron by resplicing at exon-exon junctions. *Mol Cell* **2:** 787–796. doi:10.1016/S1097-2765(00)80293-2

Herzel L, Straube K, Neugebauer KM. 2018. Long-read sequencing of nascent RNA reveals coupling among RNA processing events. *Genome Res* **28:** 1008–1019. doi:10.1101/gr.232025.117

Hörz W, Altenburger W. 1981. Sequence specific cleavage of DNA by micrococcal nuclease. *Nucleic Acids Res* **9:** 2643–2658. doi:10.1093/nar/9.12.2643

Hoskins RA, Landolin JM, Brown JB, Sandler JE, Takahashi H, Lassmann T, Booth BW, Zhang D, Wan KH, Yang L, et al. 2011. Genome-wide analysis of promoter architecture in *Drosophila melanogaster*. *Genome Res* **21:** 182–192. doi:10.1101/gr.112466.110

Hsin JP, Manley JL. 2012. The RNA polymerase II CTD coordinates transcription and RNA processing. *Genes Dev* **26:** 2119–2137. doi:10.1101/gad.200303.112

James Kent W, Sugnet CW, Furey TS, Roskin KM, Pringle TH, Zahler AM, Haussler D. 2002. The human genome browser at UCSC. *Genome Res* **12:** 996–1006. doi:10.1101/gr.229102

Ji J-Y, Squirrell JM, Schubiger G. 2004. Both Cyclin B levels and DNA-replication checkpoint control the early embryonic mitoses in *Drosophila* Jun-Yuan. *Development* **131:** 401–411. doi:10.1242/dev.00944

Jonkers I, Kwak H, Lis JT. 2014. Genome-wide dynamics of Pol II elongation and its interplay with promoter proximal pausing, chromatin, and exons. *Elife* **3:** e02407. doi:10.7554/eLife.02407

Joseph B, Kondo S, Lai EC. 2018. Short cryptic exons mediate recursive splicing in *Drosophila*. *Nat Struct Mol Biol* **25:** 365–371. doi:10.1038/s41594-018-0052-6

Kent WJ, Zweig AS, Barber G, Hinrichs AS, Karolchik D. 2010. BigWig and BigBed: enabling browsing of large distributed datasets. *Bioinformatics* **26:** 2204–2207. doi:10.1093/bioinformatics/btq351

Keren H, Lev-Maor G, Ast G. 2010. Alternative splicing and evolution: diversification, exon definition and function. *Nat Rev Genet* **11:** 345–355. doi:10.1038/nrg2776

Khodor YL, Rodriguez J, Abruzzi KC, Tang CHA, Marr MT, Rosbash M. 2011. Nascent-seq indicates widespread cotranscriptional pre-

mRNA splicing in *Drosophila*. *Genes Dev* **25:** 2502–2512. doi:10 .1101/gad.178962.111

Khodor YL, Menet JS, Tolan M, Rosbash M. 2012. Cotranscriptional splicing efficiency differs dramatically between *Drosophila* and mouse. *RNA* **18:** 2174–2186. doi:10.1261/rna.034090.112

Kwak H, Fuda NJ, Core LJ, Lis JT. 2013. Precise maps of RNA polymerase reveal how promoters direct initiation and pausing. *Science* **339:** 950–953. doi:10.1126/science.1229386

Kwasnieski JC, Orr-Weaver TL, Bartel DP. 2019. Early genome activation in *Drosophila* is extensive with an initial tendency for aborted transcripts and retained introns. *Genome Res* **29:** 1188–1197. doi:10.1101/gr.242164.118

Larson MH, Mooney RA, Peters JM, Windgassen T, Nayak D, Gross CA, Block SM, Greenleaf WJ, Landick R, Weissman JS. 2014. A pause sequence enriched at translation start sites drives transcription dynamics in vivo. *Science* **344:** 1042–1047. doi:10 .1126/science.1251871

Laver JD, Marsolais AJ, Smibert CA, Lipshitz HD. 2015. Regulation and function of maternal gene products during the maternal-to-zygotic transition in *Drosophila*. *Curr Top Dev Biol*. **113:** 4384. 10 .1016/bs.ctdb.2015.06.007

Lee JEA, Mitchell NC, Zaytseva O, Chahal A, Mendis P, Cartier-Michaud A, Parsons LM, Poortinga G, Levens DL, Hannan RD, et al. 2015. Defective Hfp-dependent transcriptional repression of *dMYC* is fundamental to tissue overgrowth in *Drosophila* XPB models. *Nat Commun* **6:** 7404. doi:10.1038/ncomms8404

Li H, Handsaker B, Wysoker A, Fennell T, Ruan J, Homer N, Marth G, Abecasis G, Durbin R. 2009. The Sequence Alignment/Map format and SAMtools. *Bioinformatics* **25:** 2078–2079. doi:10.1093/ bioinformatics/btp352

Lott SE, Villalta JE, Schroth GP, Luo S, Tonkin LA, Eisen MB. 2011. Noncanonical compensation of zygotic x transcription in early *Drosophila melanogaster* development revealed through single-embryo RNA-seq. *PLoS Biol* **9:** e1000590. doi:10.1371/journal.pbio.1000590

Lund E, Dahlberg JE. 1992. Cyclic 2′, 3′-phosphates and nontemplated nucleotides at the 3′ end of spliceosomal U6 small nuclear RNAs. *Science* **255:** 327–330. doi:10.1126/science.1549778

Martin M. 2011. Cutadapt removes adapter sequences from high-throughput sequencing reads. *EMBnet.J* **17:** 10–12. doi:10.14806/ ej.17.1.200

Martin RM, Rino J, Carvalho C, Kirchhausen T, Carmo-Fonseca M. 2013. Live-cell visualization of pre-mRNA splicing with single-molecule sensitivity. *Cell Rep* **4:** 1144–1155. doi:10.1016/j.celrep .2013.08.013

Martinho RG, Guilgur LG, Prudêncio P. 2015. How gene expression in fast-proliferating cells keeps pace. *Bioessays* **37:** 514–524. doi:10 .1002/bies.201400195

Maslon MM, Braunschweig U, Aitken S, Mann AR, Kilanowski F, Hunter CJ, Blencowe BJ, Kornblihtt AR, Adams IR, Cáceres JF. 2019. A slow transcription rate causes embryonic lethality and perturbs kinetic coupling of neuronal genes. *EMBO J* **38:** e101244. doi:10.15252/embj.2018101244

Mayer A, Di Iulio J, Maleri S, Eser U, Vierstra J, Reynolds A, Sandstrom R, Stamatoyannopoulos JA, Churchman LS. 2015. Native elongating transcript sequencing reveals human transcriptional activity at nucleotide resolution. *Cell* **161:** 541–554. doi:10 .1016/j.cell.2015.03.010

Morris DP, Greenleaf AL. 2000. The splicing factor, Prp40, binds the phosphorylated carboxyl-terminal domain of RNA polymerase II. *J Biol Chem* **275:** 39935–39943. doi:10.1074/jbc.M004118200

Nojima T, Gomes T, Grosso ARF, Kimura H, Dye MJ, Dhir S, Carmo-Fonseca M, Proudfoot NJ. 2015. Mammalian NET-seq reveals genome-wide nascent transcription coupled to RNA processing. *Cell* **161:** 526–540. doi:10.1016/j.cell.2015.03.027

Nojima T, Gomes T, Carmo-Fonseca M, Proudfoot NJ. 2016. Mammalian NET-seq analysis defines nascent RNA profiles and associated RNA processing genome-wide. *Nat Protoc* **11:** 413–428. doi:10.1038/nprot.2016.012

Nojima T, Rebelo K, Gomes T, Grosso AR, Proudfoot NJ, Carmo-Fonseca M. 2018. RNA polymerase II phosphorylated on CTD serine 5 interacts with the spliceosome during co-transcriptional splicing. *Mol Cell* **72:** 369–379.e4. doi:10.1016/j.molcel.2018.09.004

Pai AA, Henriques T, McCue K, Burkholder A, Adelman K, Burge CB. 2017. The kinetics of pre-mRNA splicing in the *Drosophila* genome and the influence of gene architecture. *Elife* **6:** e32537. doi:10.7554/eLife.32537

Pai AA, Paggi JM, Yan P, Adelman K, Burge CB. 2018. Numerous recursive sites contribute to accuracy of splicing in long introns in flies. *PLoS Genet* **14:** e1007588. doi:10.1371/journal.pgen .1007588

Pertea M, Pertea GM, Antonescu CM, Chang TC, Mendell JT, Salzberg SL. 2015. StringTie enables improved reconstruction of a transcriptome from RNA-seq reads. *Nat Biotechnol* **33:** 290–295. doi:10.1038/nbt.3122

Pritchard DK, Schubiger G. 1996. Activation of transcription in *Drosophila* embryos is a gradual process mediated by the nucleocytoplasmic ratio. *Genes Dev* **10:** 1131–1142. doi:10.1101/gad.10 .9.1131

Proudfoot NJ. 2016. Transcriptional termination in mammals: stopping the RNA polymerase II juggernaut. *Science* **352:** aad9926. doi:10.1126/science.aad9926

Prudêncio P, Rebelo K, Grosso AR, Martinho RG, Carmo-fonseca M. 2020. Analysis of mammalian native elongating transcript sequencing (mNET-seq) high-throughput data. *Methods* **178:** 89–95. doi:10.1016/j.ymeth.2019.09.003

Quinlan AR, Hall IM. 2010. BEDTools: a flexible suite of utilities for comparing genomic features. *Bioinformatics* **26:** 841–842. doi:10.1093/bioinformatics/btq033

Ramírez F, Ryan DP, Grüning B, Bhardwaj V, Kilpert F, Richter AS, Heyne S, Dündar F, Manke T. 2016. deepTools2: a next generation web server for deep-sequencing data analysis. *Nucleic Acids Res* **44:** W160–W165. doi:10.1093/nar/gkw257

Reimer KA, Mimoso CA, Adelman K, Neugebauer KM. 2021. Co-transcriptional splicing regulates 3′ end cleavage during mammalian erythropoiesis. *Mol Cell* **81:** 998–1012.e7. doi:10.1016/j.molcel .2020.12.018

Robberson BL, Cote GJ, Berget SM. 1990. Exon definition may facilitate splice site selection in RNAs with multiple exons. *Mol Cell Biol* **10:** 84–94. doi:10.1128/MCB.10.1.84

Rothe M, Pehl M, Taubert H, Jäckle H. 1992. Loss of gene function through rapid mitotic cycles in the *Drosophila* embryo. *Nature* **359:** 156–159. doi:10.1038/359156a0

Sandler JE, Irizarry J, Stepanik V, Dunipace L, Amrhein H, Stathopoulos A. 2018. A developmental program truncates long transcripts to temporally regulate cell signaling. *Dev Cell* **47:** 773–784.e6. doi:10.1016/j.devcel.2018.11.019

Saunders A, Core LJ, Sutcliffe C, Lis JT, Ashe HL. 2013. Extensive polymerase pausing during *Drosophila* axis patterning enables high-level and pliable transcription. *Genes Dev* **27:** 1146–1158. doi:10 .1101/gad.215459.113

Schlackow M, Nojima T, Gomes T, Dhir A, Carmo-Fonseca M, Proudfoot NJ. 2017. Distinctive patterns of transcription and RNA processing for human lincRNAs. *Mol Cell* **65:** 25–38. doi:10 .1016/j.molcel.2016.11.029

Schulz KN, Bondra ER, Moshe A, Villalta JE, Lieb JD, Kaplan T, McKay DJ, Harrison MM. 2015. Zelda is differentially required for chromatin accessibility, transcription factor binding, and gene expression in the early *Drosophila* embryo. *Genome Res* **25:** 1715–1726. doi:10.1101/gr.192682.115

Sheridan RM, Fong N, D'Alessandro A, Bentley DL. 2019. Widespread backtracking by RNA Pol II is a major effector of gene activation, 5′ pause release, termination, and transcription elongation rate. *Mol Cell* **73:** 107–118.e4. doi:10.1016/j.molcel.2018.10.031

Shermoen AW, O'Farrell PH. 1991. Progression of the cell cycle through mitosis leads to abortion of nascent transcripts. *Cell* **67:** 303–310. doi:10.1016/0092-8674(91)90182-X

Sousa-Luís R, Dujardin G, Zukher I, Kimura H, Weldon C, Carmo-Fonseca M, Proudfoot NJ, Nojima T. 2021. POINT technology illuminates the processing of polymerase-associated intact nascent transcripts. *Mol Cell* **81:** 1935–1950.e6. doi:10.1016/j.molcel.2021.02.034

Sterner DA, Carlo T, Berget SM. 1996. Architectural limits on split genes. *Proc Natl Acad Sci* **93:** 15081–15085. doi:10.1073/pnas.93.26.15081

Veloso A, Kirkconnell KS, Magnuson B, Biewen B, Paulsen MT, Wilson TE, Ljungman M. 2014. Rate of elongation by RNA polymerase II is associated with specific gene features and epigenetic modifications. *Genome Res* **24:** 896–905. doi:10.1101/gr.171405.113

Virtanen P, Gommers R, Oliphant TE, Haberland M, Reddy T, Cournapeau D, Burovski E, Peterson P, Weckesser W, Bright J, et al. 2020. SciPy 1.0: fundamental algorithms for scientific computing in Python. *Nat Methods* **17:** 261–272. doi:10.1038/s41592-019-0686-2

Vizcaya-Molina E, Klein CC, Serras F, Mishra RK, Guigó R, Corominas M. 2018. Damage-responsive elements in *Drosophila* regeneration. *Genome Res* **28:** 1852–1866. doi:10.1101/gr.233098.117

Wan Y, Anastasakis DG, Rodriguez J, Palangat M, Gudla P, Zaki G, Tandon M, Pegoraro G, Chow CC, Hafner M, et al. 2021. Dynamic imaging of nascent RNA reveals general principles of transcription dynamics and stochastic splice site selection. *Cell* **184:** 2878–2895.e20. doi:10.1016/j.cell.2021.04.012

Windhager L, Bonfert T, Burger K, Ruzsics Z, Krebs S, Kaufmann S, Malterer G, L'Hernault A, Schilhabel M, Schreiber S, et al. 2012. Ultrashort and progressive 4sU-tagging reveals key characteristics of RNA processing at nucleotide resolution. *Genome Res* **22:** 2031–2042. doi:10.1101/gr.131847.111

Yan D, Neumüller RA, Buckner M, Ayers K, Li H, Hu Y, Yang-Zhou D, Pan L, Wang X, Kelley C, et al. 2014. A regulatory network of *Drosophila* germline stem cell self-renewal. *Dev Cell* **28:** 459–473. doi:10.1016/j.devcel.2014.01.020

Yeo G, Burge CB. 2004. Maximum entropy modeling of short sequence motifs with applications to RNA splicing signals. *J Comput Biol* **11:** 377–394. doi:10.1089/1066527041410418

Yuan K, Seller CA, Shermoen AW, Farrell PHO. 2016. Timing the *Drosophila* mid-blastula transition: a cell cycle-centered view. *Trends Genet* **32:** 496–507. doi:10.1016/j.tig.2016.05.006

Zhu L, Zhang Y, Zhang W, Yang S, Chen J-Q, Tian D. 2009. Patterns of exon-intron architecture variation of genes in eukaryotic genomes. *BMC Genomics* **10:** 47. doi:10.1186/1471-2164-10-47

MEET THE FIRST AUTHORS

Pedro Prudêncio

Rosina Savisaar

Kenny Rebelo

Meet the First Author(s) is a new editorial feature within *RNA*, in which the first author(s) of research-based papers in each issue have the opportunity to introduce themselves and their work to readers of *RNA* and the RNA research community. Pedro Prudêncio, Rosina Savisaar, and Kenny Rebelo are co-first authors of this paper, "Transcription and splicing dynamics during early *Drosophila* development." Pedro is a postdoctoral fellow at the Institute of Molecular Medicine, Lisbon in the lab of Dr. Carmo-Fonseca, with a focus on the interplay between transcription and splicing. Rosina is also a postdoctoral fellow in the Carmo-Fonseca group, with an interest in the kinetics of splicing and how it is linked to the evolution of splicing regulatory information. Kenny is a molecular genetics graduate student at the University of Toronto in the lab of Benjamin Blencowe, with an interest in understanding how nuclear protein complexes process RNA to enable cellular function.

What are the major results described in your paper and how do they impact this branch of the field?

In this paper, we brought the NET-seq method out of the cell dish and into whole *Drosophila* embryos (*d*NETseq), allowing us to explore several aspects of RNA biology in this model. We studied transcription termination and found evidence that this process may exhibit mechanistic differences depending on whether the transcription unit is isolated or overlaps a convergent gene. As genes expressed earlier in embryonic development are more likely to be isolated, this means that preferred mechanisms of transcription termination may evolve as development progresses. We also addressed problems of splicing kinetics. We observed that many introns are spliced immediately after transcription, including very large introns, suggesting that splicing via intron definition is not limited to small introns.

Continued

What led you to study RNA or this aspect of RNA science?

PP: My desire is to understand the complex regulation of gene expression. I started my scientific career working in *Drosophila* embryogenesis in Rui Martinho's lab, where we came across an observation that led to questions that we didn't have the tools to answer. Luckily, and in collaboration with the Carmo-Fonseca lab, I had the opportunity to learn this incredible technique and to adapt it to *Drosophila* embryos, and with this, have the chance to look at gene expression from a perspective never done before in this system.

RS: Splicing is incredibly complex and incredibly confusing to study, and this is what always attracted me to the field. For my PhD, I worked on the molecular evolution of splicing signals. Several groups, including the Carmo-Fonseca lab, were making fascinating novel findings regarding the kinetics of splicing. I became curious as to how the dynamic nature of splicing was affecting these evolutionary processes, and hence decided to focus on splicing kinetics for my postdoctoral work.

KR: Fascination over how similar organized and regulated biological processes can be to assembly lines in a factory. I joined the Carmo-Fonseca lab during my M.Sc. where I was able to explore this interest when analyzing data that opened the cell's "factory door" to study transcription and splicing.

During the course of these experiments, were there any surprising results or particular difficulties that altered your thinking and subsequent focus?

RS: A *d*NETseq experiment gives rise to a bottomless treasure trove of information. However, the analysis required to convert that information into insight is complex and wrought with perils. For instance, an increase in the transcription initiation rate, a decrease in the elongation rate, and a phosphorylation hotspot can all lead to similar signatures in the sequencing data, and one must be very careful to keep all of these alternatives in mind when performing the analysis. Being confronted with the complexity of this data has made me realize how much more insight I could gain if I had a larger toolkit for my analyses. I have thus sought out training in more advanced statistical modeling techniques, something that I may have never done if I had not encountered *d*NETseq data.

PP: Exploring the features of nascent RNA with *d*NETseq requires a significant amount of biological sample. This made the analysis of earlier *Drosophila* developmental stages as planned extremely difficult. We therefore focused on later stages of development. However, NET-seq data is so full of information that we still ended up revealing several exciting new features of RNA transcription and processing.

What are some of the landmark moments that provoked your interest in science or your development as a scientist?

KR: I was impressed, in more than one unique moment, by my colleagues' readiness to adapt and produce solutions when confronted with unexpected or confounding results. By constantly challenging myself and keeping an open mind, I aspire to match this problem-solving ability, which is core to spearheading your own research.

If you were able to give one piece of advice to your younger self, what would that be?

KR: Develop a professional and efficient communication method. I believe this is one of the most pertinent skill sets to establish early on because it can work to proactively avoid misunderstandings. For example, when presenting an idea to a colleague or your supervisor be sure to not imply that your idea is better and instead explain the results/evidence to guide the other person to connect the same dots that you did.

What are your subsequent near- or long-term career plans?

RS: I am currently looking for ways to keep on doing the kinds of things that scientists do, but as a freelancer, away from the classical academic career path. This is so as to have more flexibility with regard to where in the world I can live but also to be able to take on more diverse projects. My primary interest at the moment is in methods for teaching statistics, and I am in the process of organizing a gargantuan statistics course at my institute. Exciting times!

PP: The field has exciting open questions, and although technology is developing exponentially, different techniques are still pointing in different directions. This means that there is still work to be done in the field to understand how these incredible and complex macromolecules that synthesize and modify RNA are regulated. Taking advantage of the latest technology to analyze these processes, I expect to use the next years of my postdoc to explore these features in more detail and specifically in the context of a multicellular organism.

What were the strongest aspects of your collaboration as co-first authors?

This was an amazing collaboration, primarily because our backgrounds are so complementary. Each of us was learning new things in every conversation that we had.

RNA

A PUBLICATION OF THE RNA SOCIETY

Transcription and splicing dynamics during early *Drosophila* development

Pedro Prudêncio, Rosina Savisaar, Kenny Rebelo, et al.

Supplemental Material	http://rnajournal.cshlp.org/content/suppl/2021/10/19/rna.078933.121.DC1
References	This article cites 103 articles, 30 of which can be accessed free at: http://rnajournal.cshlp.org/content/28/2/139.full.html#ref-list-1
Open Access	Freely available online through the *RNA* Open Access option.
Creative Commons License	This article, published in *RNA*, is available under a Creative Commons License (Attribution 4.0 International), as described at http://creativecommons.org/licenses/by/4.0/.
Email Alerting Service	Receive free email alerts when new articles cite this article - sign up in the box at the top right corner of the article or **click here.**